Permian post-collisional basic magmatism from Corsica to the Southeastern Alps

Andrea Boscaini [a,*], Andrea Marzoli [a,1], Joshua F.H.L. Davies [b,2], Massimo Chiaradia [b], Hervé Bertrand [c], Alberto Zanetti [d], Dario Visonà [a], Angelo De Min [e], Fred Jourdan [f,g]

[a] Dipartimento di Geoscienze, Università di Padova, Padova 35131, Italy
[b] Section des Sciences de la Terre, Université de Genève, Rue des Maraichers 13, 1205 Genève, Switzerland
[c] Univ Lyon, ENSL, Univ Lyon 1, CNRS, LGL-TPE, F-69007, Lyon, France
[d] Istituto di Geoscienze e Georisorse, Consiglio Nazionale della Ricerca IGG-CNR, Pavia 27100, Italy
[e] Dipartimento di Matematica e Geoscienze, Università di Trieste, Via E. Weiss, 8, 34127 Trieste, Italy
[f] School of Earth and Planetary Sciences, Curtin University, GPO Box U1987, Perth, WA 6845, Australia
[g] Western Australian Argon Isotope Facility & JdL Centre, Curtin University, GPO Box U1987, Perth, WA 6845, Australia

ARTICLE INFO

Keywords:
Permian
Post-collisional magmatism
Corsica
Alps
Variscan orogeny
Zircon

ABSTRACT

Post-Variscan Early Permian magmatism is widespread from Corsica to the Eastern Alps. After the formation of the Variscan orogenic belt between Laurussia and Gondwana, felsic and mafic bodies were emplaced during an extensional tectonic phase. This study focuses on a mafic dyke swarm that intruded in the region of Ajaccio (Corsica, France) and on a gabbroic intrusive complex outcropping in the Eastern Alps (Bressanone/Brixen, South Tyrol, Italy) both of which were emplaced during this extensional event. New U-Pb data from zircon show that both of these intrusions were emplaced at ca. 282 Ma. Most Ajaccio dykes display a calc-alkaline affinity and are characterized by enrichment of LILE (Large Ion Lithophile Elements) and LREE over HREE (Light and Heavy Rare Earth Elements) and HFSE (Nb, Ta, Hf, Zr; High Field Strength Elements). Two dykes show tholeiitic affinity and are characterized by marked LREE and Th-U depletion and by minor negative Nb-Ta anomalies on multi-element diagrams, which is typical for within-plate basalts. Bressanone/Brixen gabbros display similar geochemical features to the Ajaccio calc-alkaline samples with LREE enrichment over MREE (Medium Rare Earth Elements) and HREE, and HFSE depletion. Such characteristics are also confirmed by trace element data obtained by LA-ICP-MS on clinopyroxene and plagioclase crystals.

The calc-alkaline to tholeiitic dykes are characterized by enriched to depleted Sr-Nd-Pb isotopic compositions, respectively. Some Ajaccio dykes and the Bressanone/Brixen gabbros are clearly affected by crustal contamination. However, the combination of trace element and isotopic variations suggests that mantle source heterogeneities were also involved. Isotopic compositions of the Ajaccio dykes reveal the presence of two distinct mantle source signatures: an enriched mantle (EM) component, which dominates the composition of the calc-alkaline-like suite, while a DMM (Depleted MORB Mantle) component dominates the source of the tholeiitic suite. The EM mantle source likely formed during Variscan subduction, however the composition of the tholeiitic suite requires a source composed dominantly of depleted mantle, with a minor contribution from both the subducting slab and supra-subduction mantle wedge. The mantle source of the tholeiitic magmas possibly originated from greater depths (compared to the calc-alkaline-like suite) during the post-orogenic extensional phase potentially due to break-off and/or roll-back of the Variscan slab or mantle flow from the front or margins of the subducted slab. Notably, coeval Permian mafic intrusive bodies from throughout Corsica (Bocca di Tenda, Porto, Pila Canale) and from the Australpine and Southalpine Alps intruded at a similar time and have geochemical features that are very similar to the Ajaccio dyke swarm and Brixen gabbro. This indicates that a widespread Permian magmatic province developed in a post-orogenic extensional tectonic setting at the margin of the former Variscan belt. During the Middle-Late Triassic magmatism with similar enriched geochemical signatures occurred in the Southern Alps, Dinarides, Australpoine domains and at the end of the Triassic over central Pangea (Central Atlantic Magmatic Province). This would highlight the importance that the Variscan orogeny had in the development of a more fertile mantle.

* Corresponding author at: Dipartimento di Geoscienze, Università di Padova, via Gradenigo 6, 35131 Padova, Italy.
E-mail address: andrea.boscaini@phd.unipd.it (A. Boscaini).
[1]Permanent address: Dipartimento Territorio e Sistemi Agro-Forestali, Università di Padova, 35020 Legnaro, Italy
[2]Permanent address: Département des sciences de la Terre et de l'atmosphère, Université du Québec à Montréal, 201, avenue du Président-Kennedy, Montréal, Québec, H2X 3Y7, Canada

1. Introduction

The last stages of an orogenic system may be characterized by magmatic activity immediately post-dating the main collisional event and persisting for several million years (Turner et al., 1992). The post-collisional and post-orogenic magmatism produced in such scenarios is usually characterized by relatively depleted isotopic compositions, bimodal magmatism (acidic and basic) and shoshonitic to tholeiitic affinities compared to the previous *syn*-collisional magmatism (e.g., Bonin et al., 1998; Dokuz et al., 2019; Guo et al., 2015).

Post-collisional magmatism may be directly linked to the collapse of the orogenic belt and its lithospheric roots at the end of an orogenic cycle (e.g. Rey et al., 2001), resulting in extensional tectonics, thinning of the lithosphere and decompression melting of the rising asthenosphere (Bonin et al., 1998). Slab break-off events may occur during these phases, which lead to the rise of hot mantle from depth (Davies and von Blanckenburg, 1995). In such late- or post-orogenic environments, melting of the mantle may also occur due to poloidal or toroidal mantle flow rising from the front or margins of the subducted slab (Brombin et al., 2019; Faccenna et al., 2011). The composition of the post-orogenic magmas may preserve the signature of the subduction, which persists in the remnants of the mantle wedge. Alternatively, the magmas may record new mantle domains that have melted during the extensional regime (Zheng, 2019 and references therein).

Extensive post-collisional rift-related magmatism developed during the latest Carboniferous to early Permian throughout the entire European Variscan domain, e.g. in the Alps (Petri et al., 2017; Rottura et al., 1998; Schaltegger and Brack, 2007; Zanetti et al., 2013), the Iberian Peninsula (e.g., Pereira et al., 2014), the French Massif Central (e.g., Poilvet et al., 2011), the German Basin (e.g., Hoffmann et al., 2013), England (e.g., Hamilton and Pearson, 2011), the North Sea (e.g., Heeremans et al., 2004) and the Oslo Rift (e.g., Neumann et al., 2004). This first phase of post-collisional magmatism was followed by a second phase of widespread magmatism during the Ladinian to Norian (Middle-Late Triassic) in the southern Alps (e.g., Ivrea Zone, Dolomites, Australpine Karawanken Massif; Bellieni et al., 2010; Zanetti et al., 2013; De Min et al., 2020). Finally, during the latest Triassic tholeiitic basaltic magmas of the Central Atlantic Magmatic Province (CAMP) were emplaced over most of central Pangea (Callegaro et al., 2014; Davies et al., 2017; Marzoli et al., 2019).

This study focuses on a mafic dyke swarm that intruded the Corsica-Sardinia batholith in the region of Ajaccio (Corsica, France) and on the gabbro-diorite masses associated with the Bressanone/Brixen granodiorite pluton located in North-eastern Italy (South Tyrol). New U-Pb ages constrain the emplacement age of these mafic dykes and plutons, while whole-rock major and trace element analyses, and Sr-Nd-Pb isotopic compositions combined with modelling highlight variations in the geochemical signature and petrogenesis of this magmatism. The studied intrusions are also compared to other magmatic events in the widespread European Variscan domain in order to improve the general understanding of the post-orogenic evolution of the Variscan belt and the evolution of different mantle domains at the northern margin of Gondwana.

2. Geodynamic and geological setting

2.1. General geodynamic context

Subduction of the Medio-European oceanic crust beneath the Armorica microplate began during the Silurian-Devonian (Matte, 2001), which lead to collision between Armorica and Gondwana during the Devonian-Carboniferous (Rossi et al., 2009). Extensional tectonics developed during the Late Carboniferous, accommodating crustal re-equilibration (Faure et al., 2005), classically referred to as orogenic collapse (Rey et al., 2001). The collapse of the collisional belt at the end of orogenic cycles is usually associated with the formation of extensional detachment faults and core complexes (Froitzheim et al., 2008; Whitney et al., 2013), opening of sedimentary basins (Cassinis et al., 1995), lithospheric thinning, increasing of the crustal geothermal gradient, partial melting of the asthenospheric mantle and production of calc-alkaline to tholeiitic magmatism (Bonin et al., 1998). This tectonic phase may also be associated with break-off of the subducting slab and to poloidal up-flow of deep mantle from the front of the subducted lithosphere (e.g., Brombin et al., 2019; Faccenna et al., 2011). Variscan deformation culminated during the Early Carboniferous (Läufer et al., 2001) and at the end of the orogenesis the direction of the belt was oriented *E*-W to WSW-ENE (Matte, 2001; Ziegler et al., 1997). During the Permo-Carboniferous, the beginning of subduction of the Palaeotethys plate beneath Eurasia and the Variscan chain progressively transformed the western convergent margin into a diffuse dextral transform margin associated with transtension, crustal thinning, intrusive and effusive magmatic activity, and strike-slip basins (Cassinis et al., 2012). Muttoni et al. (2003), on the basis of palaeomagnetic data, described a "Pangea B" configuration in which Gondwana is located ca. 3000 km east with respect to Laurasia, as usually described in the "Pangea A" configuration (Van der Voo, 1993). The transformation from "Pangea B" to "Pangea A" occurred during the Early Permian due to a dextral megashear between Gondwana and Laurussia (Muttoni et al., 2003).

2.2. Corsica

The Corsica batholith can be divided into three main groups of intrusions, formed at different times and characterized by distinct petrographic and mineralogical features (Fig. 1a). The first intrusion group consists of Mg-K-rich calc-alkaline granites, exposed in the western and north-western areas of Corsica. These intrusions are referred to as "U1 intrusions" after Orsini (1980). They are mainly composed of quartz monzonites and monzogranites and were dated at 344 ± 2 Ma to 335 ± 4 Ma (zircon Pb-evaporation ages; Paquette et al., 2003; Rossi and Cocherie, 1995).

The second group of intrusions is the most common and comprises the "U2 association" of Orsini (1980). Most of these rocks are granodiorites and monzonites, but tonalites and gabbros are also present. All of the U2 intrusions were formed over a short period of time, from ca. 305 to 290 Ma (e.g. Pila Canale, Casta, Malfacu granodiorites, 304 ± 2 Ma, 303 ± 6 Ma, 302 ± 3 Ma, respectively; zircon Pb-Pb-evaporation ages from Rossi and Cocherie, 1995). Basic intrusions are usually slightly younger than the acid and intermediate intrusions, with ages of ca. 290–280 Ma. Gabbros in Pila Canale and Levie have been dated at 279.2 ± 0.6 Ma and 285.2 ± 0.6 Ma respectively (U-Pb zircon by ID-TIMS; Paquette et al., 2003). The youngest suite of intrusions is the "U3 metaluminous and alkaline granites". These granitoids are exposed in the Elvisa, Bonifatto, Tolla, Bavella and Popolasca massifs (Rossi and Cocherie, 1995). The ages for these rocks are 282.9 ± 1.1 Ma and 259 ± 6 Ma (U-Pb zircon and Sm-Nd mineral isochrons respectively; Poitrasson et al., 1998).

2.3. North-East Italy (South Tyrol)

In the Southern Alps (Fig. 1b) large volumes of Permian volcanics (the Athesian Volcanic district; Rottura et al., 1998) are rimmed by coeval plutons, i.e. M. Sabion, M. Croce, (Kreuzberg), Ivigna (Ifinger), Bressanone/Brixen to the northwest and Cima d'Asta to the south (Bellieni et al., 2010). The volcanism occurred simultaneously with the deposition of the Ponte Gardena conglomerates (290.7 ± 3 Ma, U-Pb zircon SHRIMP; Visonà et al., 2007) and ended at 274.1 ± 1.6 Ma, (U-Pb zircon; Marocchi et al., 2008) with the formation of large calderas and eruption of rhyolitic ignimbrites in the Bolzano/Bozen area. The volcanic lava piles reached a thickness of ~2000 m, most of which was acidic in composition, although andesites and basaltic andesites are also common (Bellieni et al., 2010; Marocchi et al., 2008). In the plutonic sequences, mafic rocks (diorites and gabbros) are scarce, and usually form small, dismembered bodies scattered within the acidic plutons

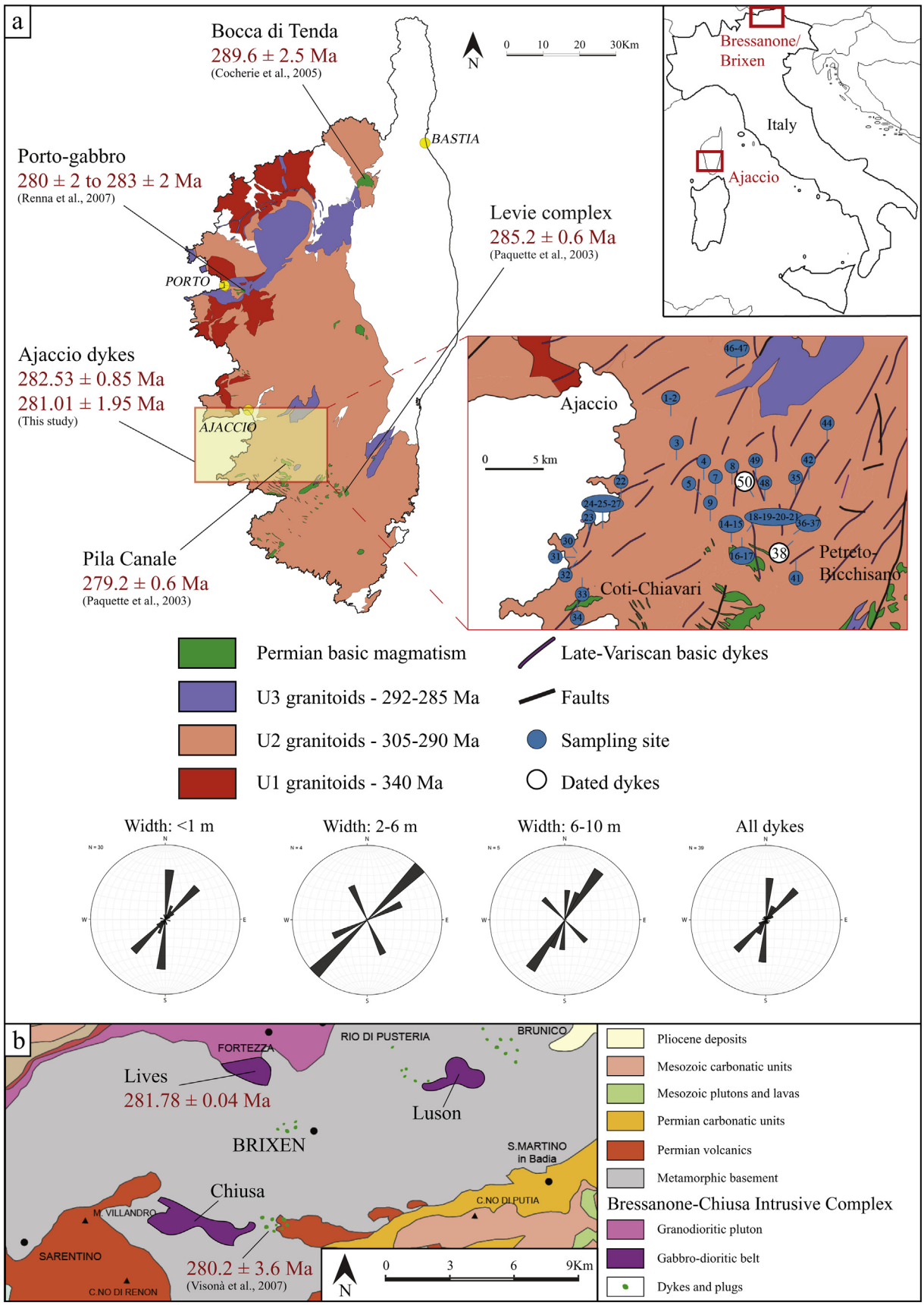

Fig. 1. (a) Simplified geological map of the Corsica batholith, sampling sites (modified after Carmignani and Rossi, 2000) and rose diagrams illustrating strike-directions of the sampled dykes in the region of Ajaccio. (b) Simplified geological map of the igneous complex of Brixen-Chiusa (modified after Geological-Structural map of Trentino 1:10000). GPS coordinates of the samples are reported in Table A1 in the supplementary material. (For interpretation of the references to colour in this figure legend, the reader is referred to the web version of this article.)

showing localized mingling with the coeval felsic magmas. The diorites and gabbros from the Bressanone/Brixen or Lives (Brixen hereafter) area represent an exception and form a distinct belt south of the Brixen granodioritic pluton. Together they constitute the Brixen-Chiusa/Klausen Intrusive Complex (Visonà, 1995). The Brixen granodiorite is a composite pluton emplaced into the metamorphic basement at about 10 km depth (Wyhlidal et al., 2012). It consists mainly of granodiorites and minor S-type cordierite-hypersthene granites (Rottura et al., 1998). The gabbro-dioritic belt (Visonà, 1995), which crop out immediately south of the pluton, is composed of three major bodies (Brixen, Luson/Lüsen and Chiusa/Klausen; Rottura et al., 1998), and a swarm of dykes and plugs (Fig. 1b). Diorites are the most common, followed by (in decreasing abundance) quartz-gabbros, scarce monzodiorites, granodiorites and granites. The acidic and mafic igneous bodies have identical ages, i.e. 282 ± 14 Ma for the Brixen granodiorites (Rb/Sr whole-rock isochron; Del Moro and Visonà, 1982) and 280.2 ± 3.6 Ma for andesitic necks near Klausen/Chiusa (U-Pb zircon SHRIMP; Visonà et al., 2007).

3. Sampling

For this study, mafic dykes were sampled in southwestern Corsica, in the region between Ajaccio, Coti-Chiavari and Petreto Bicchisano (Fig. 1a). Despite widespread alteration, most dykes yield fresh cores, which were targeted in this study and all intruded into the U2 granitic unit of the Variscan Corsica batholith, whose grain size, mineral assemblage and composition are highly variable. The width of the dykes is variable: most are less than 1 meter wide, but numerous 2–3-meter-wide dykes are also present as well as a few 10 m wide dykes.

Fig. 1a shows the distribution of all the sampled Ajaccio dykes, with a N-S trend and N45E dip. Among the larger dykes (6–10 m thickness) three are oriented N50E to N60E, one is N-S, and one ca. N60W. There is no significant difference between the orientation of intermediate (2–6 m) and thin (<1-meter) dykes.

In Northern Italy, gabbroic rocks were sampled from the southern portion of the magmatic complex of Brixen (South Tyrol), in the Scheindenberg-Lufiskofel area (Monte del Bersaglio and Dosso Lives) (Fig. 1b). The basic intrusion covers an area of about 12 km^2 and the rocks range from coarse-grained (cm-sized crystals of pyroxene and plagioclase), to fine-grained. Mineral layering with cumulus texture is locally observed. Brixen gabbros are similar to gabbroic rocks from gabbro-dioritic belt, the nearby Lüsen/Luson, Chiusa/Klausen bodies and related dykes (Visonà, 1995 and references therein).

4. Analytical methods

Analytical methods are briefly described here; complete descriptions can be found as supplementary material.

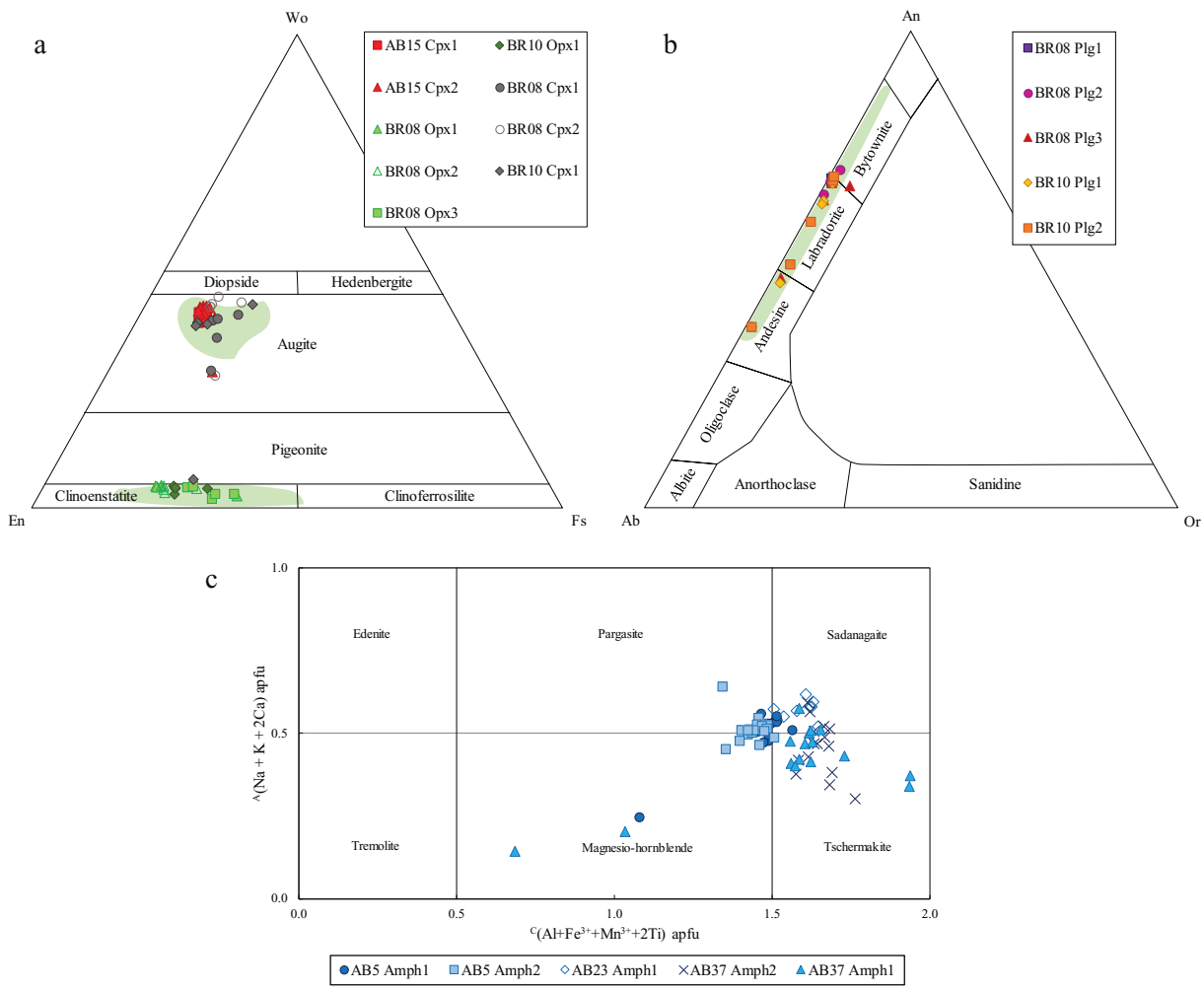

Fig. 2. Classification diagrams for the minerals from the Ajaccio dykes (AB samples) and Brixen gabbroic complex (BR samples). (a) Triangular plot for clinopyroxenes classification (Morimoto et al., 1988). (b) Triangular plot for plagioclase feldspar classification. (c) Classification diagram for amphiboles (Locock, 2014). Green fields: data for Brixen and nearby gabbros from Visonà (1995). (For interpretation of the references to colour in this figure legend, the reader is referred to the web version of this article.)

Whole-rock major element and selected trace element contents were determined by X-ray fluorescence (XRF) at the University of Padova with a Philips PW2400 spectrometer, following methods described in Callegaro et al. (2014). Analytical uncertainties range from 1% to 2% for major elements and from 10% to 15% for trace elements. Trace elements were also analysed by Inductively Coupled Plasma–Mass Spectrometry (ICP-MS) at the University of Bretagne Occidentale at Brest (France), following the analytical protocols described in Barrat et al. (1996).

Sr, Nd and Pb radiogenic isotope ratios were measured at the Department of Earth Sciences (University of Geneva, Switzerland) using a Thermo Neptune PLUS Multi-Collector ICP-MS following the method described in detail in Chiaradia et al. (2011) and Béguelin et al. (2015).

Mineral major element compositions were obtained by electron microprobe analysis (CAMECA SX50) at the CNR-IGG, Padova (Italy) following methods described in Marzoli et al. (2019).

The trace element concentrations of the minerals were determined by LA-ICP-MS at the IGG-C.N.R., Pavia using a PerkinElmer SCIEX ELAN DCR-e quadrupole ICP-MS coupled to a Q-switched Nd:YAG laser source, model Brilliant (Quantel), following the methods described in Miller et al. (2012).

U-Pb geochronology was conducted at the Universities of Geneva and Lausanne (Switzerland). At the Institute of Earth Sciences at the University of Lausanne, zircons from Ajaccio samples were analysed using a Thermo ELEMENT XR sector field ICP-MS coupled to a UP-193FX ArF excimer laser ablation system (following methods described by Ulianov et al., 2012). U-Pb zircon analyses on the Brixen samples were conducted in Geneva lab with an IsotopX PHOENIX thermal ionisation mass spectrometer (TIMS) using the techniques described by Davies et al. (2017).

5. Petrography and mineral compositions

5.1. Petrography

Ajaccio samples are porphyritic to glomerophyric with phenocrysts of plagioclase (40–60%) and clinopyroxene (30–40%) in variable concentrations; amphibole and Fe-Ti oxides are also present in lower abundances (5–10%). The groundmass is typically aphanitic and made of clinopyroxene and plagioclase. Five Ajaccio samples are phaneritic and contain large (up to 1.5–2 mm) euhedral to subhedral crystals of clinopyroxene and plagioclase (and sometimes primary amphibole). Other samples contain abundant plagioclase (50–70%) and less abundant clinopyroxene (10–20%). In several cases, plagioclase is affected by sericitic alteration, which can be pervasive in some samples. Two Ajaccio samples (AB14 and AB15) are phaneritic and contain abundant phenocrysts of euhedral to subhedral clinopyroxene (50–70%) and minor plagioclase (10–20%), which are less altered compared to other samples. Opaque minerals (titanomagnetite and rare ilmenite) are common in all Ajaccio dykes (5–10%).

Brixen gabbros mainly contain clinopyroxene (30–40%), orthopyroxene (10–20%), plagioclase (50–60%), secondary amphibole and minor secondary biotite and less abundant interstitial quartz (<5%), locally displaying granophyric texture when paired with alkali feldspar. Heavily altered olivine is present in some samples, however it can still be recognized due to the crystal shape and due to the alteration minerals (mainly iddingsite). Generally, fine-grained samples are allotriomorphic and are pervasively altered. Coarse-grained samples are hypiodiomorphic to idiomorphic. They tend to be less altered than fine-grained samples and characterized by abundant pyroxene and zoned plagioclase.

5.2. Mineral compositions

Clinopyroxene crystals from sample AB15 in Ajaccio plot in the augite field (Fig. 2a; Morimoto et al., 1988). They have an augitic composition ($Wo_{39–41}$ $En_{49–47}$ $Fs_{12–12}$) and Mg# (molar 100 x Mg / [Mg + Fe], where Fe is total iron) of ~70, with no significant variation from core to rim. Amphibole crystals from sample AB5 plot in the Mg-hornblende and pargasite fields, while crystals from samples AB23 and AB37 plot in the sadanagaite field and in the tschermakite field, respectively (Fig. 2c; Locock, 2014).

Clinopyroxene crystals from Brixen gabbros BR08 and BR10 are augites (Fig. 2a; $Wo_{37–40}$ $En_{46–44}$ $Fs_{17–15}$ and Wo_{33} En_{50} Fs_{17},

Fig. 3. Pyrolite (Hofmann, 1988) normalized and Chondrite (McDonough and Sun, 1995) normalized trace element and REE data for clinopyroxene (cpx; a) and plagioclase (plg; b) from the Brixen gabbros.

respectively) and have slightly decreasing Mg# from core to rim (Mg# = 79 to 68). These crystals have also been analysed for trace element contents. They are characterized by similar LREE and HREE contents and patterns, with depleted LREE/MREE (e.g., La/Sm_N = 0.414) and HREE/MREE (e.g., Yb/Sm_N = 0.681) and a distinct negative Eu anomaly. They also display Sr and HFSE (Zr, Hf, Ti) depletion (Fig. 3a).

The orthopyroxene crystals from the Brixen gabbro plot in the clinoenstatite field (Fig. 2a; Wo_{3-4} En_{65-72} Fs_{32-24} and Wo_4 En_{70} Fs_{26}, respectively) and have similar Mg# core-rim variations to the clinopyroxenes (Mg# = 75 to 66).

The plagioclase crystals are mostly labradorite (Fig. 2b) with core to rim zoning (An_{67} to An_{44}) observed in some samples. They display LILE and LREE enrichment (e.g., La/Sm_N = 13.078) and a strong positive Eu anomaly (Fig. 3b). Major and trace element compositions of crystals are reported in Table A2 and Table A3 in supplementary material.

6. Zircon U-Pb age determinations

Zircon crystals were successfully separated from three samples from Ajaccio (AB38, AB42, AB50) and used for U-Pb dating. Sample AB38 was collected south-east of Ajaccio, between Petreto-Bicchisano, Pila Canale

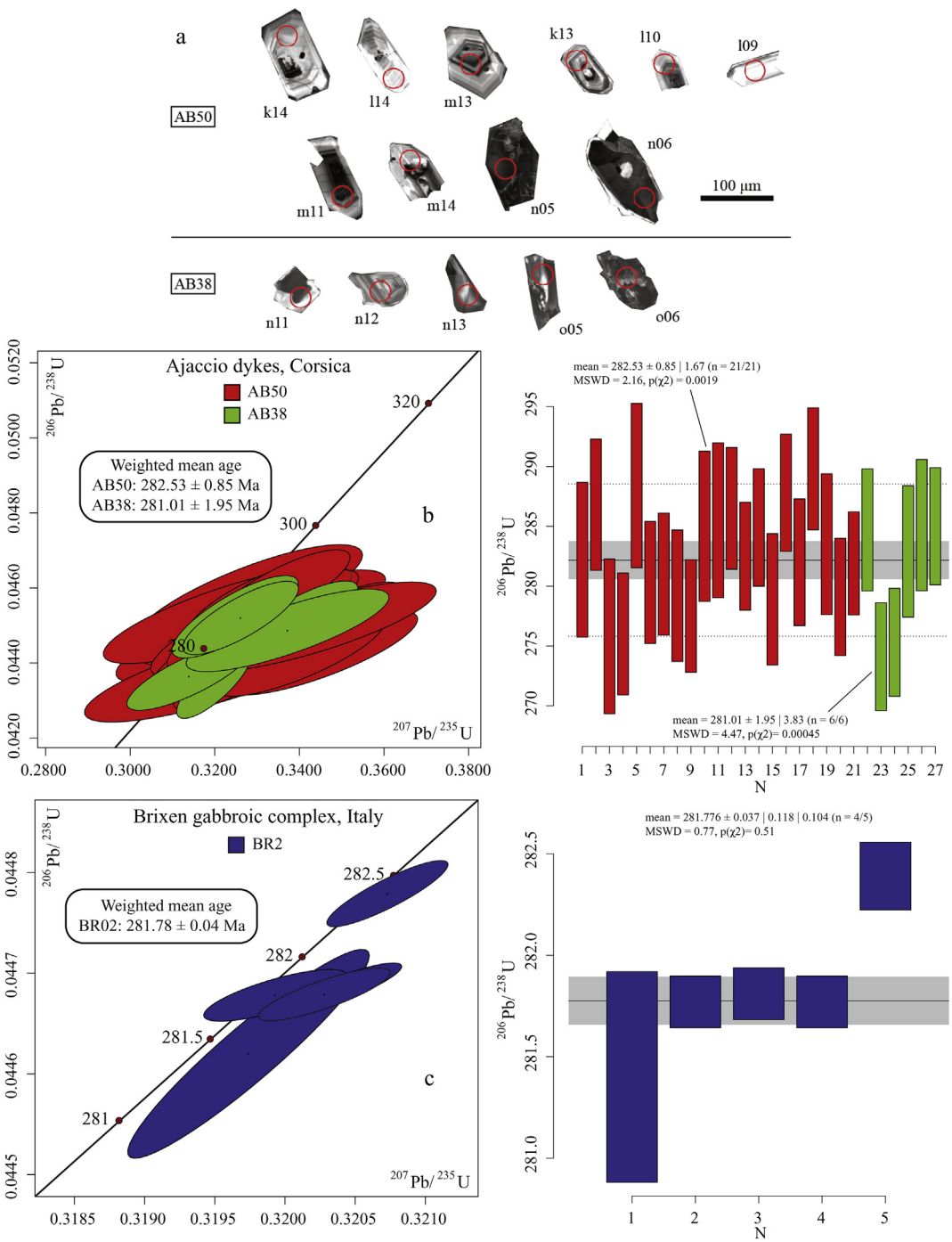

Fig. 4. U-Pb zircon ages. (a) Cathodoluminescence (CL) images of selected zircons from Ajaccio samples AB50 and AB38. (b) Concordia diagram and $^{206}Pb/^{238}U$ weighted mean age for concordant zircons from Ajaccio samples AB50 and AB38. (c) Concordia diagram and $^{206}Pb/^{238}U$ weighted mean age for concordant zircons from the Brixen gabbro BR02.

Table 1
U-Pb age data of zircons from mafic Ajaccio dykes and Brixen gabbros.

Zircon	$^{207}Pb/^{235}U$	error	$^{206}Pb/^{235}U$	error	Apparent ages, Ma			
					$^{207}Pb/^{235}U$	error	$^{206}Pb/^{235}U$	error
*Sample AB50**								
k12	0.32600	0.01200	0.04476	0.00053	284.6	8.9	282.2	3.3
k13	0.33230	0.00730	0.04551	0.00046	291.2	5.6	286.8	2.8
k14	0.32100	0.01300	0.04372	0.00053	280.0	10.0	275.8	3.3
l05	0.37390	0.00590	0.04522	0.00056	322.1	4.3	285.1	3.4
l06	0.32530	0.00620	0.04375	0.00041	285.4	4.8	276.0	2.6
l07	0.32800	0.01100	0.04576	0.00057	287.3	8.6	288.4	3.5
l08	0.33420	0.00620	0.04444	0.00043	292.3	4.7	280.3	2.6
l09	0.29000	0.01000	0.03400	0.00130	257.0	7.9	215.5	7.8
l10	0.33120	0.00780	0.04456	0.00042	289.6	5.9	281.0	2.6
l11	0.34520	0.00930	0.04427	0.00046	299.9	7.0	279.2	2.8
l12	0.32430	0.00600	0.04399	0.00039	284.7	4.6	277.5	2.4
l13	0.33100	0.01200	0.04521	0.00052	288.3	9.2	285.0	3.2
l14	0.32300	0.01200	0.04528	0.00053	282.5	9.0	285.5	3.3
m05	0.33780	0.00660	0.04545	0.00042	294.9	5.0	286.5	2.6
m06	0.33260	0.00540	0.04480	0.00037	291.1	4.1	282.5	2.3
m07	0.39590	0.00710	0.05196	0.00059	338.1	5.1	326.5	3.6
m08	0.43400	0.01600	0.04285	0.00051	363.0	11.0	270.4	3.2
m09	0.34750	0.00690	0.04518	0.00040	302.2	5.2	284.9	2.5
m10	0.34010	0.00820	0.04421	0.00045	297.0	6.1	278.9	2.8
m11	0.32960	0.00650	0.04566	0.00041	288.7	5.0	287.8	2.5
m12	0.34060	0.00800	0.04291	0.00090	296.7	6.2	270.7	5.6
m13	0.32200	0.00700	0.04472	0.00044	282.7	5.4	282.0	2.7
m14	0.33610	0.00650	0.04599	0.00042	293.6	4.9	289.8	2.6
m15	0.34300	0.01200	0.04496	0.00049	297.7	9.0	283.5	3.0
n06	0.31970	0.00590	0.04425	0.00040	281.2	4.6	279.1	2.5
n07	0.32000	0.00460	0.04470	0.00036	281.6	3.6	281.9	2.2
*Sample AB38**								
n08	0.35300	0.00560	0.04037	0.00047	306.5	4.1	255.1	2.9
n09	0.31580	0.00480	0.04205	0.00037	278.3	3.7	265.5	2.3
n10	0.33940	0.00590	0.04516	0.00042	296.3	4.5	284.7	2.6
n11	0.31980	0.00360	0.04345	0.00038	281.6	2.8	274.1	2.3
n12	0.31390	0.00600	0.04364	0.00037	277.2	4.7	275.3	2.3
n13	0.33720	0.00980	0.04487	0.00045	293.7	7.4	282.9	2.8
n14	0.32480	0.00610	0.04523	0.00045	285.1	4.7	285.1	2.8
n15	0.32010	0.00430	0.04276	0.00035	281.7	3.3	269.9	2.1
o06	0.32610	0.00560	0.04520	0.00040	286.1	4.3	285.0	2.5
o07	0.43090	0.00680	0.04273	0.00049	363.2	4.8	269.7	3.0
*Sample AB42**								
o08	0.90500	0.04900	0.04561	0.00059	636.0	28.0	287.5	3.6
*Sample BR2***								
z01	0.31974	0.22	0.044620	0.19	281.70	0.54	281.40	0.53
z02	0.31993	0.13	0.044678	0.047	281.85	0.33	281.77	0.13
z03	0.32040	0.11	0.044685	0.046	282.21	0.27	281.81	0.13
z04	0.32028	0.12	0.044679	0.048	282.12	0.30	281.77	0.13
z05	0.32073	0.11	0.044779	0.060	282.46	0.26	282.39	0.17

* The Ajaccio samples data errors are 2SE.
** The Brixen sample data errors are 2σ.

and Urbalacone. It belongs to a N20E oriented and 2 m wide basaltic dyke. Ten zircons were extracted from the sample. Sample AB50 is classified as a basaltic trachyandesite collected east of Urbalacone (see below). It belongs to a N5E oriented and 1 m wide dyke and yielded 26 zircon crystals. Sample AB42 was collected north of Urbalacone. It is a basaltic andesite and belongs to a N5E oriented, ~5 m wide dyke. Notably, the only zircon extracted from this sample yielded a strongly discordant age and therefore it will be not considered furthermore in the discussion.

Cathodoluminescence (CL) reveals that most zircons have oscillatory zoning, consistent with a magmatic origin. Grains from sample AB50 are stubby and euhedral (e.g. k13, k14, l14, m11); some have unzoned cores and zoned rims (e.g. l09), while others have zoned cores and rims (e.g. k13, k14, l10, m13). Grains from sample AB38 show no significant zoning (except grain n12) and have very low-cathodoluminescence emission (e.g. n13, o06,). Selected grains are shown in Fig. 4a.

All U-Pb zircon ages are reported in Table 1; however, some zircon grains are not concordant or are clear outliers in terms of apparent age and these are not plotted on the figure. Grains l05, l09, m08, m12 from sample AB50 (red) and grains n08, n09, n15, o07 from sample AB38 (green) have been excluded due to discordance likely related to Pb loss. Grain m07 from sample AB50 yielded a significantly older age than the rest of the concordant zircons and is interpreted as reflecting Pb inheritance. These ten zircons have been excluded from the age calculations (Fig. 4b).

21 zircons from sample AB50 yielded a $^{206}Pb/^{238}U$ weighted mean age of 282.53 ± 0.85 Ma, while the 6 zircons from sample AB38 yielded a $^{206}Pb/^{238}U$ weighted mean age of 281.01 ± 1.95 Ma. (Fig. 4b).

Sample BR02 from the Brixen gabbroic complex contained pockets with a granophyric texture, from which 5 zircons were extracted. Four out of five grains analysed by CA-TIMS (chemical abrasion Thermal Ionisation Mass Spectrometry) are concordant and yielded a $^{206}Pb/^{238}U$ weighted mean age of 281.78 ± 0.04 Ma (Fig. 4c). Ajaccio and Brixen intrusions are therefore statistically indistinguishable in age.

Table 2
Major element compositions (wt.%) of mafic Ajaccio dykes and Brixen gabbros (XRF analyses).

Location	*Ajaccio, Corsica (France)*																				
Sample	AB1	AB3	AB4	AB5	AB7	AB8	AB9	AB14	AB15	AB16	AB17	AB18	AB19	AB20	AB21	AB22	AB23	AB24	AB25	AB27	AB30
SiO_2	49.22	47.91	50.11	47.57	49.02	48.81	49.86	48.05	47.09	48.95	48.85	48.49	49.56	48.67	49.01	49.75	46.91	47.54	52.27	47.44	54.52
TiO_2	2.23	1.70	1.78	1.20	1.97	2.32	2.38	4.94	4.45	1.97	1.80	1.83	1.76	1.80	1.92	2.98	3.16	3.15	2.02	3.19	1.07
Al_2O_3	16.23	17.21	16.23	14.07	17.09	16.35	16.43	12.71	12.06	16.52	17.03	17.00	17.11	17.58	17.19	15.21	15.3	15.3	16.72	15.35	18.63
Fe_2O_3	12.17	10.78	10.45	11.36	11.12	11.66	12.59	15.50	15.85	11.43	10.70	10.75	10.41	10.64	10.94	13.77	15.01	14.45	10.79	14.57	9.20
MnO	0.17	0.17	0.18	0.15	0.17	0.15	0.20	0.19	0.19	0.17	0.16	0.16	0.16	0.16	0.16	0.18	0.2	0.21	0.15	0.2	0.15
MgO	7.44	8.10	8.69	12.78	7.44	6.82	5.93	6.68	9.11	7.91	7.56	7.39	7.18	7.70	7.16	4.64	5.34	4.99	5.24	5.21	4.89
CaO	8.08	9.63	7.91	10.26	8.74	8.44	6.26	8.41	8.19	8.84	9.58	9.71	9.39	9.69	9.65	7.16	8.1	7.66	5.89	7.37	7.48
Na_2O	3.43	3.07	3.11	1.95	3.44	3.35	4.55	2.51	2.13	3.14	2.93	3.08	2.93	2.98	3.27	3.88	3.06	3.43	4.16	3.57	2.80
K_2O	0.96	1.08	1.07	0.31	1.14	0.99	1.02	0.98	0.65	0.88	0.82	0.81	0.92	0.39	0.41	1.62	2.07	1.78	1.69	1.84	1.23
P_2O_5	0.44	0.28	0.46	0.28	0.40	0.86	0.59	0.35	0.33	0.46	0.40	0.38	0.40	0.40	0.43	0.78	0.77	0.75	0.54	0.8	0.20
Tot	100.37	99.95	100.00	99.93	100.52	99.75	99.79	100.32	100.05	100.27	99.85	99.63	99.83	100.02	100.15	99.96	99.93	99.27	99.48	99.55	100.18
L.O.I	1.96	3.45	3.37	3.61	3.99	2.62	3.79	2.03	2.28	0.86	1.38	0.96	1.27	1.35	2.05	2.86	2.62	2.90	3.80	2.99	2.95

Location	*Ajaccio, Corsica (France)*																*Brixen (Northern Italy)*			
Sample	AB31	AB32	AB33	AB34	AB35	AB36	AB37	AB38	AB41	AB42	AB44	AB46	AB47	AB48	AB49	AB50	BR4	BR8	BR9	BR10
SiO_2	48.84	47.33	52.94	50.89	49.10	48.29	48.86	49.7	49.17	53.83	56.20	50.55	50.55	50.35	49.3	53.67	53.28	54.77	54.96	55.91
TiO_2	1.93	3.13	1.78	1.75	1.77	2.93	2.76	2.44	2.30	1.13	1.40	1.56	1.67	1.79	1.71	1.47	0.67	0.65	0.69	0.83
Al_2O_3	17.26	15.45	15.75	15.83	15.08	15.6	15.65	15.92	17.71	17.70	16.71	16.58	17.47	16.50	16.83	16.77	17.61	16.54	14.24	15.80
Fe_2O_3	11.2	14.69	9.82	10.37	10.58	13.82	13.69	11.84	11.19	7.86	8.12	9.88	9.98	10.70	10.16	9.4	8.14	8.43	8.51	8.46
MnO	0.18	0.21	0.16	0.16	0.16	0.2	0.20	0.17	0.16	0.14	0.14	0.16	0.14	0.25	0.16	0.15	0.15	0.16	0.16	0.15
MgO	6.89	5.11	7.31	8.37	8.70	5.05	5.28	6.02	5.51	6.51	5.56	6.66	5.9	8.09	7.14	5.02	6.95	6.97	9.35	6.43
CaO	8.19	7.54	7.44	6.56	8.58	7.7	7.57	8.62	8.63	8.62	6.33	8.84	8.36	7.83	9.9	7.04	9.34	9.50	8.59	8.20
Na_2O	4.36	4.22	2.65	3.83	3.90	3.97	3.82	3.4	3.52	3.39	3.63	2.87	3.77	3.08	2.96	3.86	1.95	2.04	1.81	2.19
K_2O	0.65	1.06	1.51	1.53	0.87	1.28	1.38	0.95	0.87	0.76	1.70	1.96	1.28	1.05	0.88	1.47	1.30	0.97	1.51	1.52
P_2O_5	0.41	0.79	0.53	0.46	1.00	0.77	0.69	0.35	0.55	0.14	0.19	0.37	0.33	0.43	0.4	0.64	0.11	0.11	0.12	0.15
Tot	99.93	99.54	99.89	99.74	99.74	99.62	99.92	99.41	99.61	100.08	99.98	99.45	99.45	100.08	99.44	99.47	99.50	100.14	99.94	99.64
L.O.I	3.63	3.10	3.50	3.65	2.89	1.81	1.90	1.09	1.61	2.44	2.99	2.12	1.97	2.64	2.08	1.99	2.84	0.27	0.54	0.50

7. Whole-rock compositions

Whole-rock compositions of the Ajaccio dykes and Brixen gabbros are reported in Table 2 and plotted in a total alkali vs. silica diagram (TAS; Le Bas et al., 1986). Most Ajaccio samples classify as basalts and trachybasalts, while a few samples can be classified as basaltic andesites (Fig. 5). Most samples cluster above and below the line dividing the alkaline and sub-alkaline series (Irvine and Baragar, 1971). Notably, samples that are enriched in alkali elements do not show any systematic difference in terms of immobile major, minor, or trace elements compared to the rest of the samples (see below).

Based on their modal mineral compositions, the Brixen gabbros are classified as olivine-gabbros, gabbros and gabbro-norites. Plagioclase-rich rocks classify as leuco-gabbros. The whole-rock major and trace element composition of the Brixen intrusion reflects mineral accumulation and therefore can not be used to interpret their petrogenesis and is not directly comparable with the generally finer grained Ajaccio dyke samples. Nonetheless, we plotted the data from four Brixen whole-rock samples in the TAS and other diagrams (Fig. 5). Data for the Lüsen/Luson gabbro, near Brixen (Visonà, 1995) are also reported for comparison. The complete data set for Lüsen/Luson are reported in the Table A4 in the supplementary material where the analytical methods employed for these gabbros are also briefly described.

Most Ajaccio samples have similar major element compositions (Fig. 6). Exceptions are represented by sample AB5, which is significantly enriched in MgO, and samples AB14 and AB15, which are enriched in TiO_2 and $Fe_2O_{3\ tot}$ (Fig. 6a, b) and slightly depleted in Na_2O and Al_2O_3 (Fig. 6c, e), compared to the rest of the samples. In general, CaO decreases progressively with decreasing MgO (Fig. 6f). TiO_2 and Fe_2O_3 are nearly constant in primitive samples (those with MgO > 7 wt.%), while they show two distinct trends to high and low values in more evolved samples. Al_2O_3 increases slightly up to 7 wt.% MgO and decreases with more evolved compositions. Na_2O and K_2O increase with decreasing MgO.

In the Ternary AFM plot (Irvine and Baragar, 1971) most samples plot in the calc-alkaline field or next to the dividing line with the tholeiitic field (Fig. 7). Three outliers plot in the tholeiitic field: AB14 and AB15 are ferro-basalts, while AB5 is Mg-rich. Despite its apparent tholeiitic character in the AFM plot, we consider sample AB5 among the calc-alkaline samples because it shows similar major and in particular similar trace element compositions and ratios to the rest of the calc-alkaline samples (see below).

Whole-rock trace elements compositions are reported in Fig. 8 and Table 3. The tholeiitic signature of the two samples AB14 and AB15 is also confirmed by their trace element compositions, which can be distinguished from those of the rocks with calc-alkaline affinity (Fig. 1 in the supplementary material; Pearce, 1983). Calc-alkaline dykes from Ajaccio share similar patterns displaying LREE/HREE enrichment (La/Yb_N from 2.77 to 6.64) and negative Nb-Ta and Zr-Hf anomalies. AB30 and AB42 show a positive Pb anomaly. Tholeiitic Ajaccio samples AB14, AB15 display a different pattern, with depleted LREE/MREE (e.g., $La/Sm_N = 0.64$) and more fractionated HREE compared to the calc-alkaline dykes (e.g., $Yb/Sm_N = 0.36$ against 0.50, Fig. 8a). They also have negative Th-U and Pb-Sr anomalies, a positive Ti anomaly and no significant Nb anomaly.

Similar patterns to the Ajaccio calc-alkaline basalts are displayed by two whole-rock samples from the gabbroic complex of Brixen (BR08 and BR10). These samples are enriched in LREE over MREE and HREE and are characterized by negative Nb-Ta, Zr-Hf and Eu anomalies and a positive Pb anomaly. (Fig. 8b). Since the Brixen whole-rocks compositions may not be representative of magmatic liquid compositions, we used trace element data obtained on clinopyroxenes to calculate magmatic melts, assuming equilibrium conditions using the partition coefficients of Hill et al. (2000). Melts calculated from clinopyroxene display LREE-enrichment over MREE and HREE and negative HFSE (Nb, Zr, Hf) and Eu anomalies (Fig. 8c).

Initial Sr, Nd and Pb isotopic compositions recalculated to 280 Ma were obtained for twelve Ajaccio and two Brixen samples (Table 4). For the Ajaccio dykes, $^{87}Sr/^{86}Sr_i$ values range from 0.70373 to 0.70677 and are negatively correlated with Nd isotopic compositions (Fig. 9a). Sample AB30 has a quite low $^{143}Nd/^{144}Nd_i$ and high $^{87}Sr/^{86}Sr_i$ ratio compared to the rest of the samples. The two tholeiitic samples AB14 and AB15 have the highest Nd ($^{143}Nd/^{144}Nd_i = 0.512607$ and 0.512608, respectively) and the lowest Sr ($^{87}Sr/^{86}Sr_i = 0.70373$ and 0.70387)

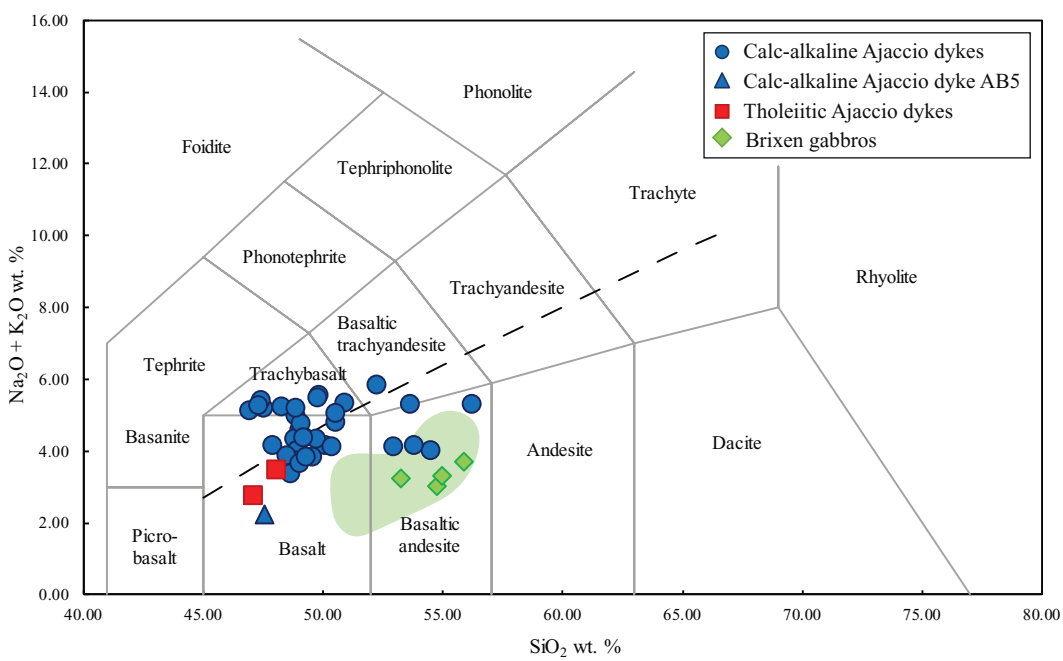

Fig. 5. Total alkali vs. silica (TAS) classification diagram (after Le Bas et al., 1986) with the Ajaccio dykes and Brixen gabbros. It should be noted that Brixen gabbros are cumulitic rocks and do not correspond to magma compositions. Green fields: data for Brixen and nearby gabbros from Visonà (1995). (For interpretation of the references to colour in this figure legend, the reader is referred to the web version of this article.)

isotopic compositions. Brixen gabbros have more radiogenic Sr and less radiogenic Nd isotopic composition ($^{143}Nd/^{144}Nd_i$ = 0.512039; $^{87}Sr/^{86}Sr_i$ = 0.70534 and 70,703) compared to the Ajaccio dykes.

Pb isotopic ratios for Ajaccio samples plot above the NHRL (Northern Hemisphere Reference Line; Hart, 1984) with $^{207}Pb/^{204}Pb_i$ from 15.609 to 15.664, $^{208}Pb/^{204}Pb_i$ from 38.061 to 38.375 and $^{206}Pb/^{204}Pb_i$ from 18.134 to 18.470 (Fig. 9b, c). The two analysed Brixen gabbros yielded similar $^{206}Pb/^{204}Pb_i$ (18.268 and 18.278) but significantly higher $^{207}Pb/^{204}Pb_i$ (15.679 and 15.680) and $^{208}Pb/^{204}Pb_i$ (18.333 and 18.436) compared to the Ajaccio dykes. Pb isotopic compositions are poorly correlated with $^{143}Nd/^{144}Nd_i$. However, a subset of Ajaccio samples shows a negative correlation of Nd vs. Pb isotopic compositions (trend 1 in Fig. 9d).

For the Ajaccio dykes, the Nd isotopic compositions are roughly correlated with trace element ratios such as La/Sm and La/Ta (Fig. 10a, b). Tholeiitic samples AB14 and AB15 plot at the depleted end of such trends, yielding the highest $^{143}Nd/^{144}Nd_i$ and the lowest values for strongly- vs moderately incompatible element ratios. For most Ajaccio calc-alkaline samples, Zr/Nb is negatively correlated with $^{206}Pb/^{204}Pb_i$ (excluding sample AB42; Fig. 10c) and positively correlated with $^{143}Nd/^{144}Nd_i$ (excluding sample AB30, low $^{143}Nd/^{144}Nd_i$; Fig. 10d).

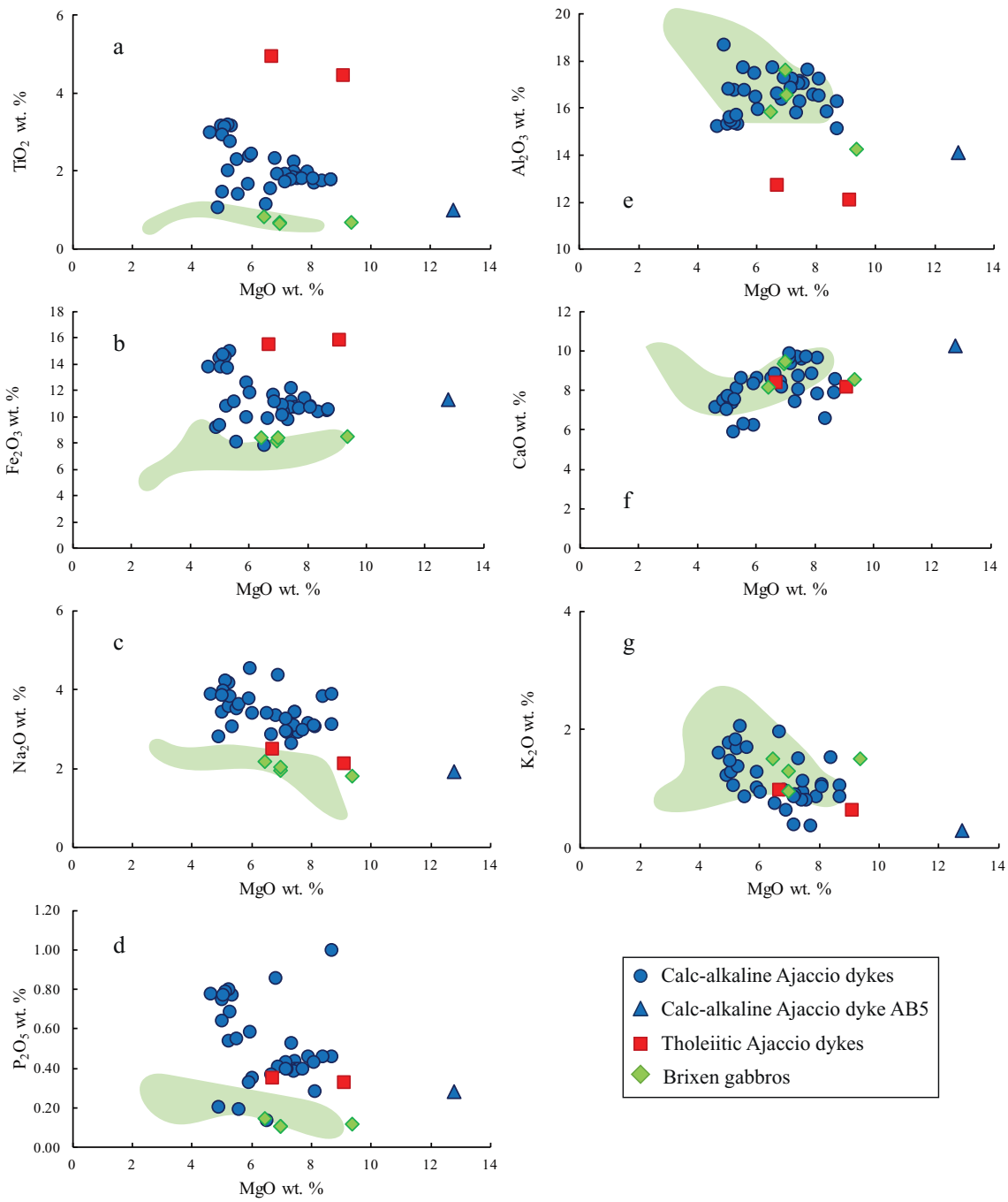

Fig. 6. Variation diagrams for selected major elements vs. MgO (wt.%). Green fields: data for Brixen and nearby gabbros from Visonà (1995). (For interpretation of the references to colour in this figure legend, the reader is referred to the web version of this article.)

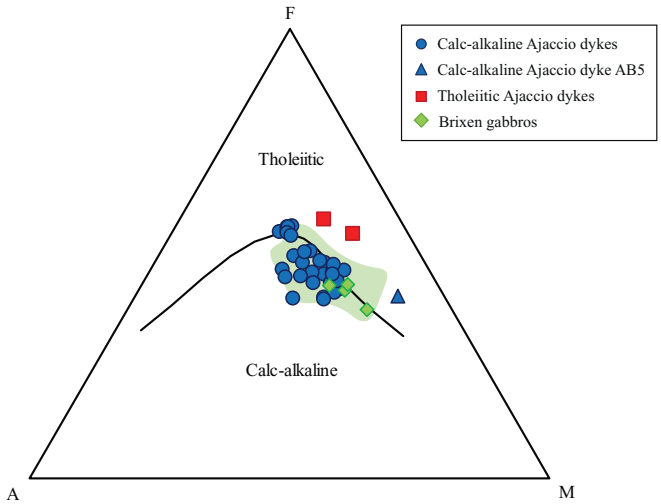

Fig. 7. Ternary AFM diagram (after Irvine and Baragar, 1971) showing Ajaccio dykes and Brixen gabbros. Green fields: data for Brixen and nearby gabbros from Visonà (1995). (For interpretation of the references to colour in this figure legend, the reader is referred to the web version of this article.)

8. Discussion

8.1. Tectonomagmatic discrimination and emplacement age

The U-Pb ages for the two calc-alkaline samples AB38 and AB50 are indistinguishable with $^{206}Pb/^{238}U$ weighted means of 281.01 ± 1.95 Ma and 282.53 ± 0.85 Ma, respectively. Assuming that these ages represent the crystallization age of all of the studied calc-alkaline dykes, we can infer that the dyke swarm in the region of Ajaccio is coeval with other mafic bodies that intruded the Corsica batholith between ca. 289 Ma and 279 Ma (i.e., Pila Canale and Levie complex, Paquette et al., 2003; basaltic dykes in southern Corsica, Traversa et al., 2003; Bocca di Tenda gabbroic rocks, Cocherie et al., 2005; Porto gabbro, Renna et al., 2007). This suggests that the early Permian mafic magmatism was widespread throughout Corsica over an area of ca. 2700 km^2 (Fig. 1) in the southern foreland of the Variscan belt after the end of the orogenic cycle (after ca. 305 Ma; Soder and Romer, 2018). The Brixen gabbro also yielded an identical weighted mean age (281.78 ± 0.04 Ma), testifying to widespread basic magmatism at ca. 280 Ma along a ca. 500 km transect from Corsica throughout the Southern Alps, from East (Brixen) to the central Alps (the Sondalo gabbro in the Austroalpine units; Petri et al., 2017; Tribuzio et al., 1999) and the western Southern

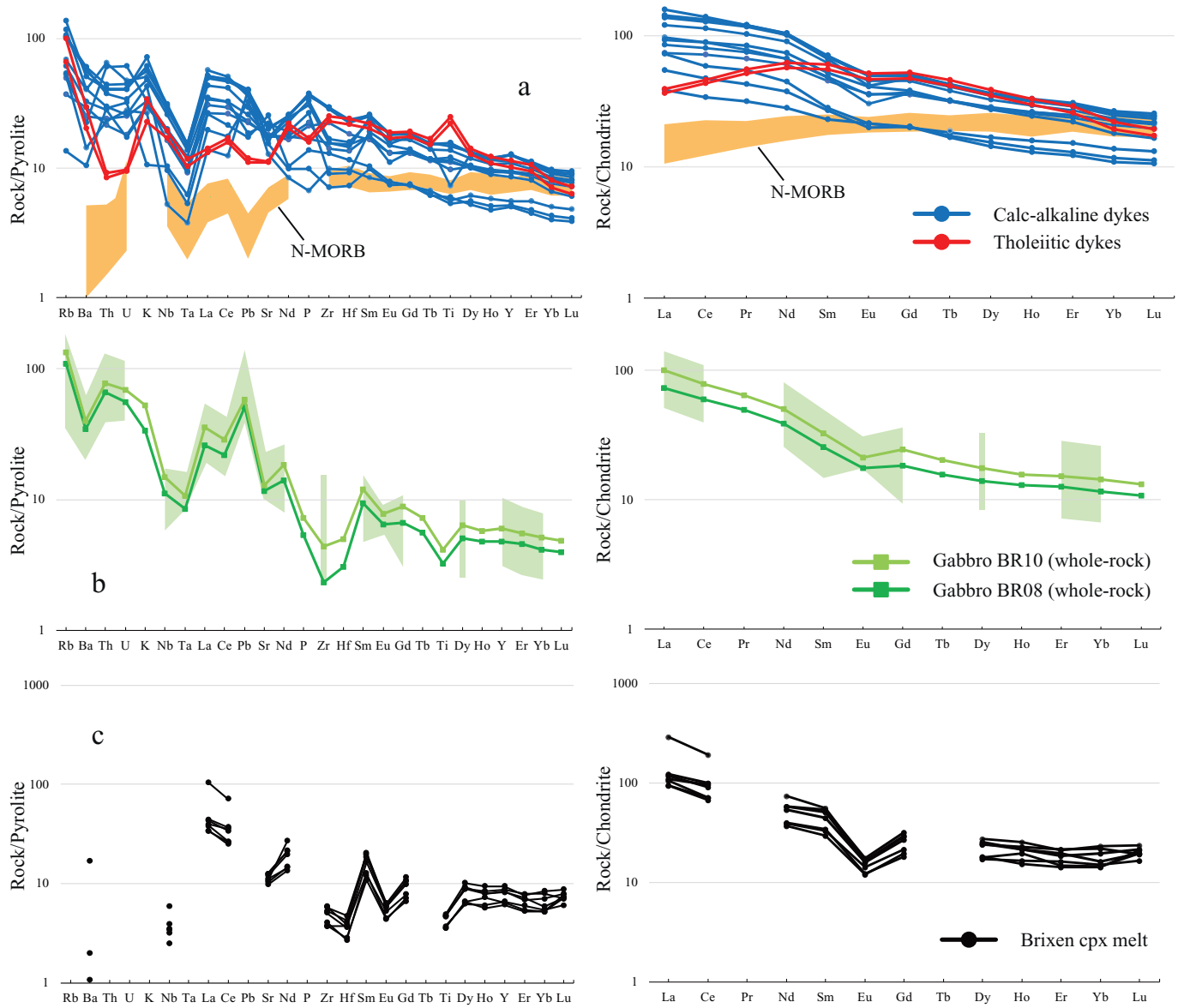

Fig. 8. Pyrolite (Hofmann, 1988) normalized and Chondrite (McDonough and Sun, 1995) normalized data for Ajaccio dykes and Brixen gabbroic complex. (a) Mafic Ajaccio dykes. Orange field: N-MORB compositions (Hofmann, 1988; Sun and McDonough, 1989). (b) Brixen whole-rock data. Green fields: data for Brixen and nearby gabbros from Visonà (1995). (c) Calculated magmatic liquid composition from trace element in Brixen clinopyroxene. (For interpretation of the references to colour in this figure legend, the reader is referred to the web version of this article.)

Table 3
Trace element whole-rock compositions (ppm) of mafic Ajaccio dykes and Brixen gabbros (ICP-MS data).

Location	*Ajaccio, Corsica (France)*														*Brixen (Northern Italy)*	
Sample	AB1	AB5	AB14	AB15	AB16	AB22	AB23	AB24	AB30	AB37	AB38	AB41	AB42	AB50	BR08	BR10
Sr	359	507	228	221	344	389	393	323	304	328	356	445	263	344	232	257
Y	39.42	21.67	49.23	43.83	39.87	54.54	54.09	54.76	22.16	46.63	40.86	36.99	23.79	48.22	20.41	25.95
Zr	236	136	265	242	149	312	301	309	74	176	165	95	103	165	24	46
Nb	10.55	6.77	12.75	11.16	12.60	19.79	19.33	20.43	6.33	17.03	13.34	13.05	3.49	18.65	7.35	9.80
Mo	1.02	0.16	0.92	0.96	0.53	1.48	1.30	1.23	0.37	1.22	0.89	0.82	0.26	0.50	–	–
Cs	1.26	0.27	0.76	1.62	1.67	1.41	1.01	0.84	1.23	0.41	1.15	2.75	0.71	0.32	3.95	8.11
Ba	164.78	68.52	192.93	134.52	194.01	395.42	369.74	334.40	270.10	388.81	147.62	215.11	94.47	264.77	228.34	263.38
La	17.42	17.34	9.26	8.69	20.18	33.67	32.59	33.72	12.94	28.43	22.85	22.20	9.17	37.39	17.13	23.57
Ce	44.15	35.88	28.39	26.53	49.43	80.71	78.26	81.38	29.19	69.45	54.38	54.61	20.90	85.35	36.72	48.30
Pr	6.24	5.03	5.16	4.76	6.99	11.14	10.87	11.23	3.95	9.60	7.27	7.77	2.92	11.21	4.62	5.97
Nd	27.64	20.47	28.21	25.94	30.66	47.39	46.35	47.62	17.01	41.18	30.37	33.91	12.89	46.03	17.60	23.11
Sm	6.73	4.19	8.98	8.24	7.21	10.37	10.20	10.48	4.02	9.18	7.06	7.70	3.40	9.86	3.79	4.90
Eu	2.03	1.21	2.89	2.62	2.01	2.86	2.78	2.84	1.13	2.56	1.71	2.31	1.20	2.36	0.99	1.19
Gd	7.07	4.05	10.39	9.48	7.36	10.09	9.90	10.00	4.06	8.99	7.25	7.58	3.95	9.47	3.62	4.80
Tb	1.14	0.61	1.66	1.51	1.17	1.55	1.51	1.53	0.63	1.38	1.17	1.16	0.66	1.47	0.56	0.72
Dy	6.88	3.54	9.56	8.59	6.92	9.01	8.73	8.91	3.77	8.06	7.01	6.75	4.13	8.65	3.40	4.30
Ho	1.42	0.71	1.81	1.62	1.39	1.80	1.74	1.77	0.76	1.60	1.44	1.33	0.86	1.73	0.71	0.86
Er	3.97	1.95	4.64	4.12	3.80	4.90	4.72	4.76	2.09	4.31	3.98	3.54	2.43	4.67	2.02	2.42
Yb	3.64	1.75	3.54	3.14	3.35	4.30	4.10	4.15	1.89	3.74	3.63	2.91	2.22	4.01	1.83	2.28
Lu	0.54	0.26	0.48	0.42	0.48	0.63	0.60	0.61	0.28	0.54	0.52	0.41	0.32	0.57	0.27	0.32
Hf	5.17	3.25	6.80	6.11	3.86	6.70	6.32	6.41	2.08	4.46	4.27	2.61	2.77	4.11	0.87	1.41
Ta	0.61	0.42	0.78	0.67	0.68	1.03	1.00	1.07	0.36	0.95	0.84	0.64	0.26	1.02	0.57	0.72
Pb	3.34	2.61	1.77	1.67	3.47	5.61	6.11	6.25	5.07	4.52	4.01	2.85	6.13	5.44	7.67	8.76
Th	1.90	2.32	0.73	0.67	1.69	3.48	3.19	3.25	2.36	2.99	4.81	2.24	1.84	5.13	5.24	6.19
U	0.51	0.65	0.20	0.19	0.37	0.90	0.82	0.83	0.53	0.69	1.24	0.35	0.57	0.96	1.13	1.40
Sc	26.18	20.27	27.24	24.92	28.68	30.63	31.79	33.35	27.08	33.80	32.24	26.12	27.21	22.72	37.16	36.75
V	201	151	463	409	208	297	327	316	210	306	312	245	165	119	208	234
Cr	172	892	188	378	242	12	16	13	26	27	77	83	170	111	588	263
Co	43.58	63.19	53.46	62.86	48.85	38.43	44.11	41.52	31.01	41.71	42.28	40.41	32.39	26.54	–	–
Ni	125.88	545.86	106.15	207.04	132.20	14.63	19.06	15.51	13.87	25.27	69.16	55.71	40.27	42.40	–	–
Rb	29.61	8.16	59.62	39.42	22.36	61.82	61.40	82.40	70.48	63.31	32.23	36.75	31.17	41.01	66.15	80.12

Alps (e.g., Ivrea gabbros; Peressini et al., 2007; Zanetti et al., 2013; Fiorentini et al., 2018).

Only two Ajaccio samples (AB14 and AB15) have a tholeiitic mid ocean ridge (MORB) affinity (Fig. 11;Hollocher et al., 2012; Wood, 1980) suggesting a different origin compared to the calc-alkaline ones. Unfortunately, no zircons were found in these dykes therefore dating them was not possible. Based on field evidence, these dykes intruded the U2 granitoids (Fig. 1; ca. 305–290 Ma), yielding a maximum crystallization age of about 290 Ma. Therefore, the tholeiitic Ajaccio dykes may be either coeval to the calc-alkaline suite in the same area (ca. 280 Ma) or related to subsequent magmatic events. Other examples of tholeiitic Permian intrusions include troctolites and gabbroic rocks from Corsica (ca. 280 Ma; Cocherie et al., 1994), the Braccia gabbro from Val Malenco, Eastern Central Alps (ca. 275 Ma; Hermann et al., 2001, and references therein) (Fig. 1 in the supplementary material), which yield similar trace element composition to the Ajaccio tholeiitic samples AB14 and AB15 (Fig. 3l in the supplementary material). Moreover, Permian Ivrea gabbros are considered as tholeiitic based on their clinopyroxenes REE patterns (Zanetti et al., 2013) and their MORB-like isotopic compositions (Voshage et al., 1990). In the nearby regions, post-Permian magmatism is represented chiefly by the Middle-Late Triassic magmatism in the Southern Alps, Australpine domain and Dinarides (ca. 240 Ma; Zanetti et al., 2013; Lustrino et al., 2019; De Min et al., 2020), and by the CAMP activity (ca. 201 Ma), which is widespread in southwestern Europe and northwestern Africa (e.g., Callegaro et al., 2014; Marzoli et al., 2019) and may have occurred also in the Ivrea

Table 4
Sr-Nd-Pb isotopic compositions of selected samples from mafic Ajaccio dykes and Brixen gabbroic complex. Initial values are recalculated to 280 Ma.

	$^{87}Sr/^{86}Sr$	$^{87}Sr/^{86}Sr_i$	$^{143}Nd/^{144}Nd$	$^{143}Nd/^{144}Nd_i$	εNd_i	$^{206}Pb/^{204}Pb$	$^{207}Pb/^{204}Pb$	$^{208}Pb/^{204}Pb$	$^{206}Pb/^{204}Pb_i$	$^{207}Pb/^{204}Pb_i$	$^{208}Pb/^{204}Pb_i$
Ajaccio											
AB1	0.70486	0.70390	0.51267	0.51240	2.33389	18.564	15.632	38.583	18.134	15.609	38.061
AB5	0.70497	0.70478	0.51259	0.51236	1.65156	18.881	15.663	38.967	18.182	15.626	38.157
AB14	0.70672	0.70373	0.51296	0.51261	6.42292	18.658	15.681	38.737	18.342	15.664	38.355
AB15	0.70593	0.70387	0.51296	0.51261	6.45253	18.620	15.655	38.646	18.300	15.638	38.283
AB16	0.70519	0.70443	0.51257	0.51231	0.56769	18.581	15.653	38.668	18.287	15.638	38.225
AB23	0.70703	0.70516	0.51256	0.51231	0.72537	18.621	15.658	38.712	18.252	15.639	38.243
AB30	0.70946	0.70677	0.51239	0.51212	−3.02089	18.566	15.660	38.722	18.284	15.645	38.308
AB37	0.70698	0.70475	0.51258	0.51233	1.03213	18.746	15.662	38.841	18.330	15.640	38.250
AB38	0.70580	0.70476	0.51255	0.51229	0.28965	19.151	15.692	39.271	18.295	15.647	38.186
AB41	0.70605	0.70511	0.51257	0.51232	0.83454	18.809	15.678	39.079	18.470	15.660	38.375
AB42	0.70546	0.70413	0.51275	0.51246	3.55727	18.558	15.653	38.581	18.306	15.640	38.313
AB50	0.70631	0.70493	0.51250	0.51226	−0.27841	18.887	15.679	39.120	18.397	15.654	38.260
Brixen											
BR08	0.70852	0.70534	0.512278	0.51204	−4.65	18.276	15.680	–	18.268	15.679	38.333
BR10	0.71308	0.70703	0.512263	0.51204	−4.65	18.306	15.681	–	18.278	15.680	38.436

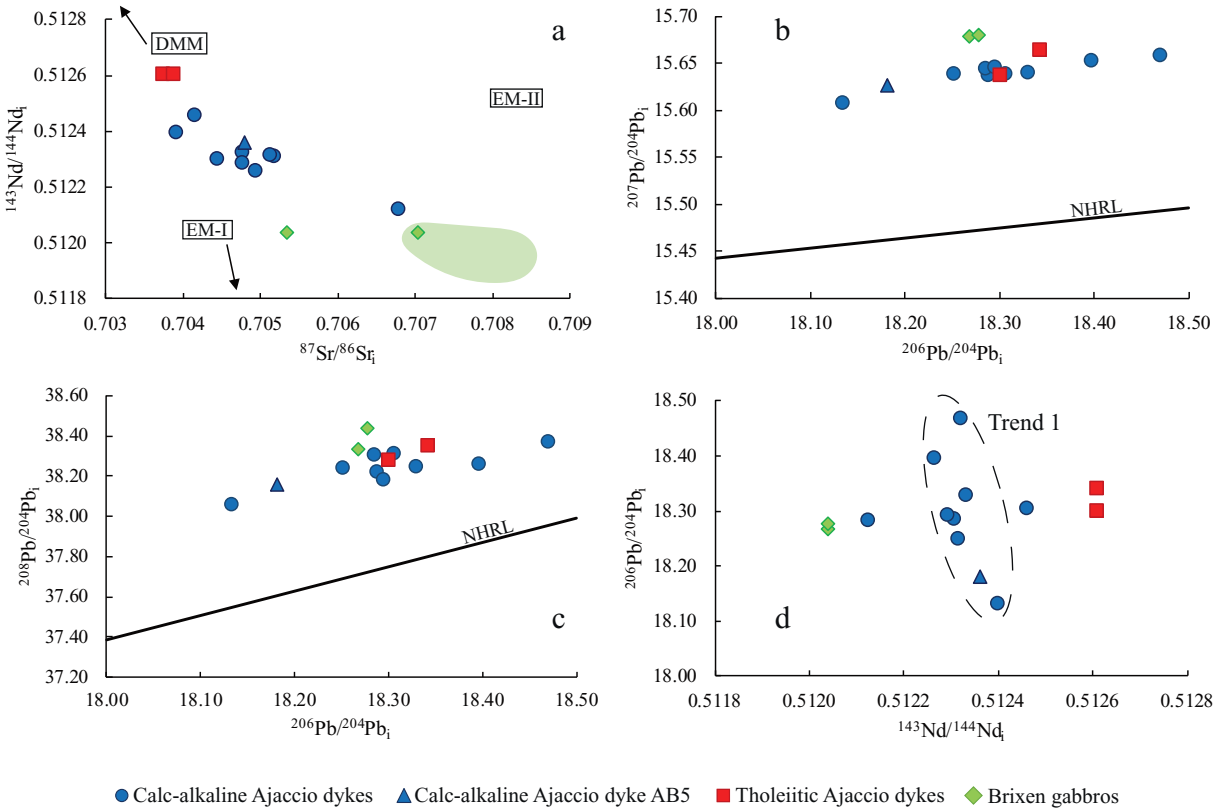

Fig. 9. Sr-Nd-Pb isotopic compositions (initial values at 280 Ma) for selected Ajaccio and Brixen samples. Green fields: data for Brixen and nearby gabbros from Visonà (1995). NHRL = Northern Hemisphere Reference Line (Hart, 1984). (For interpretation of the references to colour in this figure legend, the reader is referred to the web version of this article.)

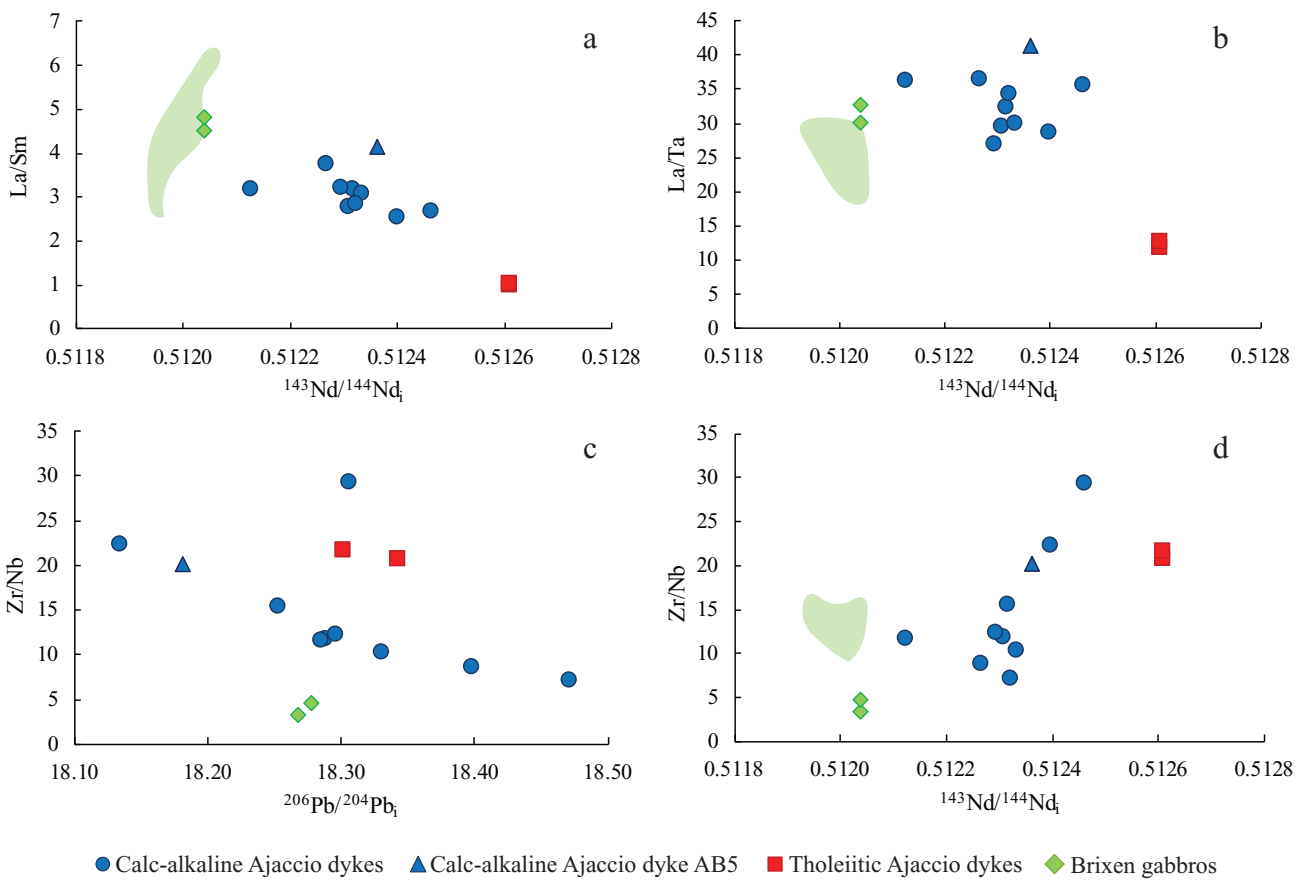

Fig. 10. Trace element ratios and Nd-Pb isotopic compositions (initial values at 280 Ma) for selected Ajaccio and Brixen samples. Green fields: data for Brixen and nearby gabbros from Visonà (1995). (For interpretation of the references to colour in this figure legend, the reader is referred to the web version of this article.)

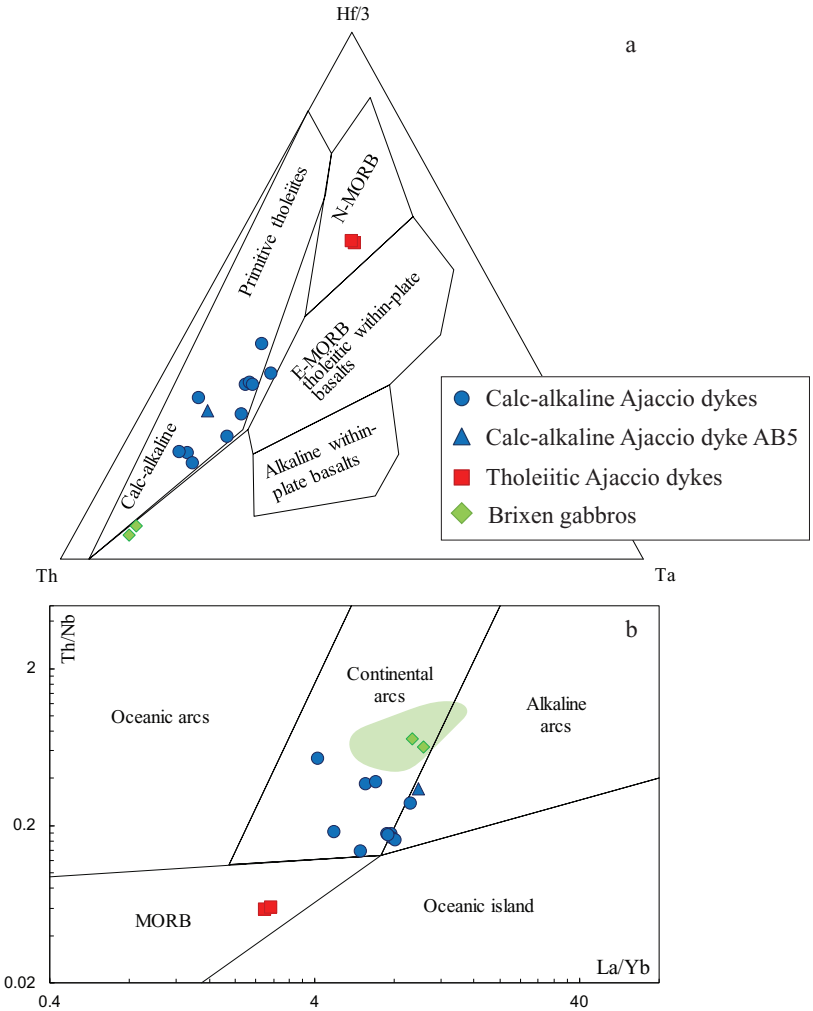

Fig. 11. Geochemical discrimination diagrams for mafic to intermediate rocks. (a) Th-Ta-Hf/3 ternary plot (Wood, 1980). (b) Th/Nb vs. La/Yb diagram (Hollocher et al., 2012). Green fields: data for Brixen and nearby gabbros from Visonà (1995). (For interpretation of the references to colour in this figure legend, the reader is referred to the web version of this article.)

zone (Denyszyn et al., 2018). However, Middle-Late Triassic magmatism is characterized by orogenic affinity acquired by deep-seated recycled crustal components (Lustrino et al.,2019; De Min et al., 2020, Casetta et al., 2018), and is chiefly alkaline to transitional in character (Casetta et al., 2018). Such Triassic magmatism is different from the Corsica tholeiites also in terms of isotopic compositions (Fig. 12). The end-Triassic CAMP basalts from southwestern Europe are different from Corsica tholeiites in terms of trace element contents and patterns as well as their Sr-Nd-Pb isotopic composition (Fig. 12; Callegaro et al., 2014; Marzoli et al., 2019). For example, all analysed CAMP rocks from Europe are low-Ti basalts ($TiO_2 < 2.0$ wt%), while the Ajaccio tholeiites are high in TiO_2 (> 4 wt%). CAMP rocks are not known, so far, from Corsica or Sardinia. In the Ivrea zone, a dunite contains zircons (most likely xenocrystic) which yielded an age close to 200 Ma (Denyszyn et al., 2018), compatible with CAMP. However, the geochemical composition of those Ivrea rocks is quite different from other European CAMP rocks as well as from Ajaccio tholeiites.

On the contrary, deep crustal gabbroic rocks from the Permian Ivrea zone (Voshage et al., 1990) bear geochemical similarities with the Corsica tholeiites, e.g., high $^{143}Nd/^{144}Nd_i$ (> 0.5126) suggesting a dominant DMM component (Fig. 12a). Permian tholeiitic dykes have been described also for southern Corsica and northern Sardinia (Traversa et al., 2003). In summary, we consider an early Permian age as the most likely also for the tholeiitic Ajaccio dykes as suggested by field and by the minor presence of Permian rocks with tholeiitic and DMM-like affinity both in Corsica and the Southern Alps (Cocherie et al., 1994; Hermann et al., 2001). Nevertheless, since we lack geochronological data for the tholeiites, we cannot exclude that calc-alkaline and tholeiitic Ajaccio intrusions may represent distinct magmatic pulses separated by several milion years (e.g., Rogers et al., 2016).

8.2. Crustal assimilation

As shown in the AFM diagram and in the trace element plots of Fig. 11 (Hollocher et al., 2012; Wood, 1980), most samples from the Ajaccio region and the Brixen gabbros have a calc-alkaline affinity and subduction signature. The subduction signature of most dykes and gabbros is in contrast with the extensional (or trans-tensional) tectonic setting in which these intrusions were emplaced ca. 20 Ma after the end of the Variscan orogeny. In this case, the subduction signature may reflect either a significant amount of crustal contamination or a previously metasomatized mantle source.

The Ajaccio dykes could have been affected by assimilation of crustal material during their intrusion or during their ascent through the crust. We used EC-AFC modelling (energy-constrained assimilation and fractional crystallization; Bohrson and Spera, 2001) to simulate the evolution of both the calc-alkaline and the tholeiitic series in terms of changing Sr-Nd isotopic ratios and trace element (Sr, Nd, Zr/Nb) compositions with increasing degrees of crustal assimilation. Sample AB1 is

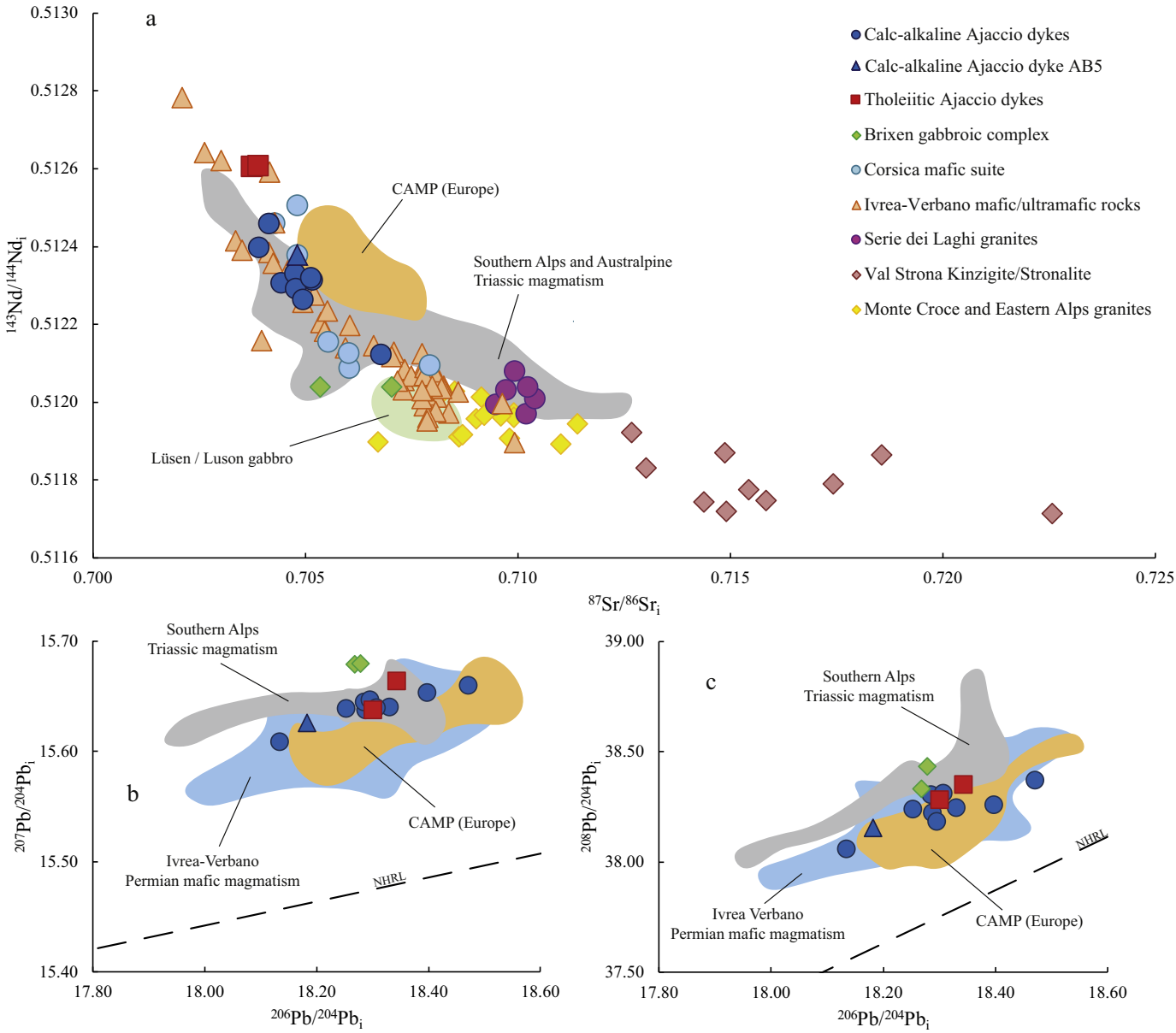

Fig. 12. Sr-Nd-Pb isotopic compositions of Permian mafic intrusions throughout the Corsica batholith and the Alps compared to the Middle-Late and end-Triassic magmatism. Ivrea-Verbano mafic-ultramafic rocks (data from Sinigoi et al., 2016, and references therein); Serie dei Laghi granites (Klötzli et al., 2014 and references therein); Monte Croce and eastern Alps Permian granites (Rottura et al., 1998 and references therein); Corsica mafic suite (Cocherie et al., 1994); Val Strona Kinzigite/Stronalite (Voshage et al., 1990); calc-alkaline and tholeiitic Ajaccio and Brixen gabbroic complex (this study). Orange field: Sr-Nd-Pb isotopic compositions of European CAMP (Cebriá et al., 2003; Callegaro et al., 2014). Grey field: Sr-Nd-Pb isotopic compositions of Middle-Late Triassic magmatism in the Southern Alps and the Australpine unit (Lustrino et al., 2019 and references therein; De Min et al., 2020). Green fields: data for Brixen and nearby gabbros from Visonà (1995). Blue field: Ivrea-Verbano Permian mafic rocks (Cumming et al., 1987). NHRL = Northern Hemisphere Reference Line (Hart, 1984). (For interpretation of the references to colour in this figure legend, the reader is referred to the web version of this article.)

considered to be representative of the parental composition for the calc-alkaline series, since it has the lowest $^{87}Sr/^{86}Sr_i$ among these samples ($^{87}Sr/^{86}Sr_i = 0.70390$), while AB14 is representative of the tholeiitic series ($^{87}Sr/^{86}Sr_i = 0.70373$). To simulate the assimilated crust, we used the composition of a Variscan granodiorite from Western Corsica (sample CLB28; Cocherie et al., 1994) dated at 312 Ma, with its Sr-Nd isotopic compositions recalculated to 280 Ma and the average Zr/Nb of the upper crust (ca. 16; Rudnick and Gao, 2003). Finally, we assumed four different values for the Sr distribution coefficient of the evolving basic magma ($Kd_{Sr} = 1.5, 0.9, 0.5, 0.1$), while the assumed Nd, Zr and Nb distribution coefficients are 0.1, 0.2 and 0.01, respectively, since they are incompatible in plagioclase (Aigner-Torres et al., 2007) and clinopyroxene (Hill et al., 2000). Modelling parameters are shown in Table 5 and the results are shown in Fig. 13.

Assuming that the chosen parameters are appropriate, the results of the EC-AFC simulation do not reproduce the general trends and evolution of the entire set of dykes. The modelling precludes any EC-AFC link between the calc-alkaline and the tholeiitic series, implying distinct parental magmas and possibly distinct mantle sources for the two suites. Accordingly, the calc-alkaline Ajaccio dykes display a positive correlation between Zr/Nb and $^{143}Nd/^{144}Nd_i$ (with one outlier; Fig. 13d). This trend is not reproduced by the assimilation of upper crust with a mean Zr/Nb ratio of ca. 16 (Rudnick and Gao, 2003) and low $^{143}Nd/^{144}Nd_i$. Therefore, heterogeneities in the mantle source are our preferred explanation for the variations in the data (as discussed below). However, among the calc-alkaline group, the modelling suggests that the samples with the highest Sr and lowest Nd isotopic compositions could be derived from the least isotopically enriched magmas

Table 5
Input parameters for EC-AFC model.

Thermal parameters of the system			Composition of magma and assimilant				
			Calc-alkaline sample AB1			*Tholeiitic sample AB14*	
Liquidus of magma (Tlm)	=	1300 °C	Element	Sr	Nd	Sr	Nd
Initial temperature of magma (Tmo)	=	1300 °C	Magma conc.	359.14	27.64	227.52	28.21
Liquidus of assimilant (Tla)	=	900 °C	Kd	1.5/0.9/0.5/0.1	0.1	1.5/0.9/0.5/0.1	0.1
Initial temperature of assimilant (Tao)	=	300 °C	Assimilant conc.	220	40	220	40
Solidus of magma and assimilant (Ts)	=	550 °C	Kd	1.5	0.1	1.5	0.1
Specific heat of magma (Cpm)	=	1484 J/Kg K	Isotope	$^{87}Sr/^{86}Sr$	$^{143}Nd/^{144}Nd$	$^{87}Sr/^{86}Sr$	$^{143}Nd/^{144}Nd$
Specific heat of assimilant (Cpa)	=	1388 J/Kg K	Ratio magma	0.703897	0.512397	0.70373	0.51261
Heat of crystallization (Hcry)	=	396,000 J/Kg	Ratio assimilant	0.707735	0.512063	0.707735	0.512063
Heat of fusion (Hfus)	=	354,000 J/Kg					

(e.g., sample AB1) through crustal assimilation (Fig. 13a, c). In this case, the amount of assimilated crust required to reach the composition of the sample with highest $^{87}Sr/^{86}Sr$ and lowest $^{143}Nd/^{144}Nd$ (i.e. sample AB50) would be ca. 40%, a highly unlikely value that would result in the basic magmas to reach andesitic composition. Contamination with older or more evolved crustal rocks (with higher Sr and lower Nd isotopic compositions) would require lower degrees of assimilation however, such rocks are unknown for Corsica, therefore EC-AFC has been attempted considering a kinzigite from the Ivrea Verbano area (sample VS10; Voshage et al., 1990). Assimilation of such rock would require a much lower amount of assimilated crust (ca. 15–20%; Fig. S2 in supplementary material). Nevertheless, even assimilation of evolved rocks such as this fails to reproduce the general trends of the calc-alkaline suite, even if it could explain the composition of some of the most evolved dykes.

The Brixen gabbros seem to have been severely affected by crustal contamination. Their enriched Sr-Nd isotopic compositions cannot be reached starting from a hypothetical calc-alkaline or tholeiitic parental magma similar to the Ajaccio dykes (e.g., similar to AB1 or AB14) combined with assimilation of Variscan granitic crust (Fig. 13a, b, c). High degrees of assimilation (ca. 30%) of a fairly evolved crustal rock (e.g., similar to the kinzigite from Ivrea Verbano area; Fig. S2 in supplementary material) would produce compositions similar to those of the Brixen gabbros. Such high degrees of contamination would produce magmas with basaltic-andesite or andesite composition and could explain why quartz crystallized in Brixen olivine-gabbros as a late magmatic phase. Gabbroic sequences from the Ivrea-Verbano (Voshage et al., 1990; Sinigoi et al., 2016) and Sondalo (Tribuzio et al., 1999) are also heavily contaminated, displaying degrees of assimilation of up to ca. 30–40% and ca. 20–40%, respectively. According to Sinigoi et al. (2016), crustal contamination is favoured in zones of deep, fertile and thick crust occurring close to the former Variscan belt like in the Ivrea or Brixen areas. On the other hand, where dyking favours a rapid passage of basic magmas through the crust, crustal contamination may be less efficient (Sinigoi et al., 2016), such as in the Ajaccio region or in the Bocca di Tenda gabbroic sequence (ca. 16–21%; Tribuzio et al., 2009).

8.3. Partial melting and fractional crystallization

In this section, we explore the melting conditions, i.e. the source mineralogy, temperature and depth, through modelling of incompatible trace elements and REE (Fig. 14). Two non-modal batch-melting curves are calculated for a garnet and for a garnet-amphibole lherzolite with primitive mantle compositions. Apart from the tholeiitic samples AB14 and AB15, all other Ajaccio samples plot just below the primitive mantle lherzolite curves and yield an apparent melting degree of 3–5%. Samples AB14 and AB15 plot at higher Dy/Yb and lower La/Yb with respect to the rest of the samples and require a more depleted mantle source composition (Fig. 14a).

Modelling was also performed with REEBOX (Table 6; Brown and Lesher, 2016). In the case of a hot harzburgite (potential temperature, TP, of 1550 °C), melting would start at ca. 4.1 GPa, while for a TP of 1450 °C melting would start at ca. 2.9 GPa. In the case of a hydrous lherzolite with a TP of 1400 °C to 1250 °C and an initial water content of 700 ppm, melting would start at ca. 5.9 to 3.7 GPa, respectively. If we assume a lithospheric thickness of 70 km, the melting column would straddle the garnet-spinel transition. All of the calc-alkaline samples are in agreement with partial melting of a lherzolite source that has a potential temperature between 1350 °C to 1250 °C with melting starting at ca. 2.9 to 2.7 GPa and variable melting degrees between ca. 1–4%. However, the tholeiitic samples AB14 and AB15 have compositions which are in agreement with melting of a depleted harzburgite source, with relatively high potential temperature between 1550 °C to 1500 °C, quite high initial melting depth (ca. 3.9 to 3.3 GPa) and an apparent melting degree of about 2% (Fig. 14a). A depleted mantle source would explain the depleted La/Sm of the tholeiites, while a high melting depth would explain the depleted HREE, i.e. a residual garnet signature.

Fractional crystallization has also been modelled considering the involvement of plagioclase and clinopyroxene in equal proportions from a basaltic melt (plagioclase- and clinopyroxene- melt partition coefficients from Aigner-Torres et al., 2007, and Hill et al., 2000, respectively). Sample AB5 (highest MgO at 12.78 wt.%) was selected as the parental magma in order to test Dy/Yb and La/Yb variations for 0 to 50% fractionation (blue curve, Fig. 14a). Only limited variations (mainly for La/Yb) are caused by the fractionation of plagioclase and clinopyroxene, whatever the composition of the parental magma. The observed variations require slightly variable melting degrees (as suggested above) or distinct mantle sources (and possibly distinct amounts of crustal assimilation).

Brixen gabbros yield similar La/Yb and slightly lower Dy/Yb compared to most of the Ajaccio dykes. With one exception, melts calculated from Brixen clinopyroxene data plot close to the Brixen whole-rock data. Such compositions are close to those of the Ajaccio calc-alkaline dykes and suggest a similar melting scenario.

8.4. Mantle source composition

As previously stated, major and trace elements and Sr-Nd-Pb isotopic compositions indicate that there are two different magmatic suites among the Ajaccio dykes. The differences between the calc-alkaline and the tholeiitic samples and the variability among the calc-alkaline group cannot be explained only as the result of magmatic processes such as crustal assimilation, low-pressure fractionation and partial melting of a homogeneous mantle source. Therefore, if we assume that the calc-alkaline and the tholeiitic suites are similar in age, a heterogeneous mantle source is suggested for the Permian.

The trace element patterns of the calc-alkaline dykes (Fig. 8a) are indicative of a subduction-related signature (Johnson and Plank, 1999). These patterns are characterized by negative anomalies in HFSE such as Nb, Ta, Hf and Zr, which are immobile elements during fluid transfer and are thus typically depleted in subduction-related magmas (Johnson and Plank, 1999). Also, the dykes are relatively enriched in LILE such as

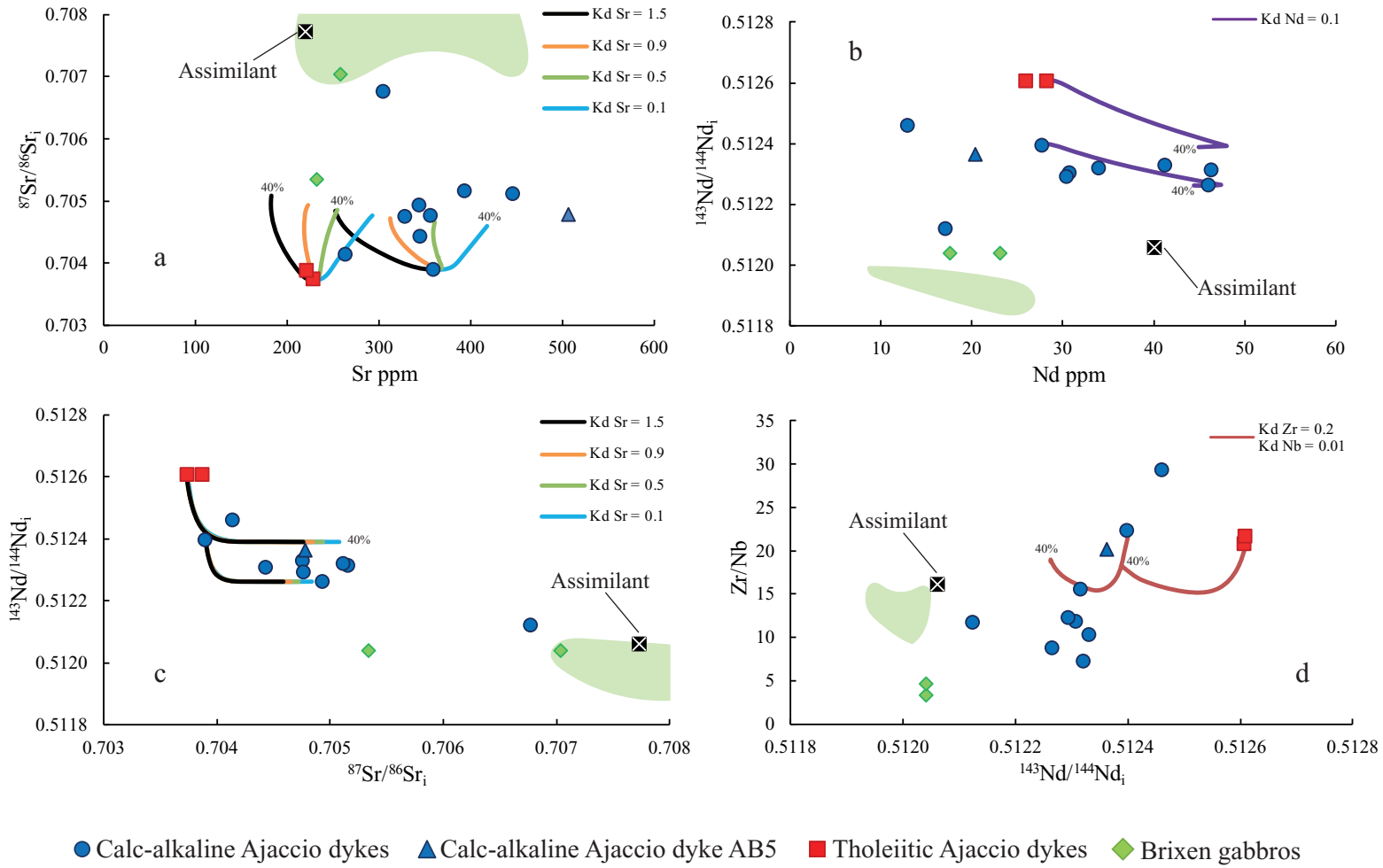

Fig. 13. EC-AFC modelling for calc-alkaline and tholeiitic Ajaccio dykes and Brixen gabbros. (a) $^{87}Sr/^{86}Sr$ vs. Sr (ppm) variation diagram for different Sr distribution coefficients (Kd_{Sr} = 1.5, 0.9, 0.5, 0.1). (b) $^{143}Nd/^{144}Nd$ vs. Nd (ppm) variation diagram for Kd_{Nd} = 0.1. (c) $^{143}Nd/^{144}Nd$ vs. $^{87}Sr/^{86}Sr$ variation diagram for different Kd_{Sr} values. (d) Zr/Nb vs. $^{143}Nd/^{144}Nd$ variation diagram for Kd_{Zr} = 0.2 and Kd_{Nb} = 0.01. The curves represent the variation of the composition of the initial magmas (sample AB1 and AB15), at increasing degree of crustal assimilation. For each diagram, crustal assimilation ranges between 0% to 40 wt.%. Green fields: data for Brixen and nearby gabbros from Visonà (1995). Parameters used in the modelling are reported in Table 5. (For interpretation of the references to colour in this figure legend, the reader is referred to the web version of this article.)

17

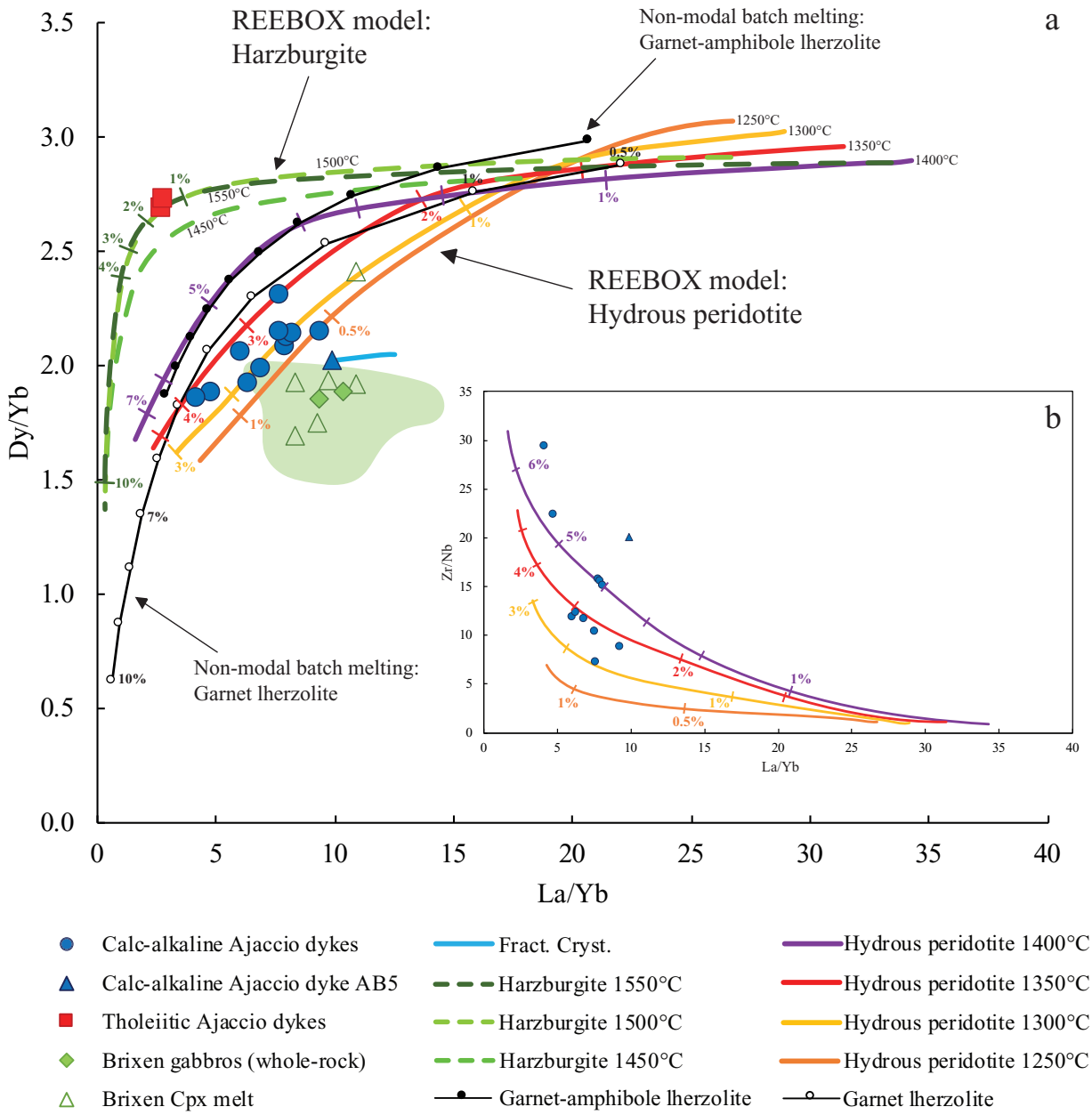

Fig. 14. Mantle-melting and fractional crystallization modelling results. Input data are reported in Table 6. a) White and black circles: non-modal batch melting curves for a garnet lherzolite (Grt-lherzolite: olivine 55 vol%, orthopyroxene 25 vol%, clinopyroxene 18 vol%, garnet 2 vol%) and for a garnet-amphibole lherzolite (Grt-amph lherzolite: olivine 55 vol%, orthopyroxene 20 vol%, clinopyroxene 17 vol%, garnet 4 vol%, amphibole 4 vol%), respectively. Coloured curves: REEBOX modelling (Brown and Lesher, 2016). The reported curves refer to the melting of different mantle sources in terms of Dy/Yb vs La/Yb variations: violet, red, yellow and orange solid lines represent a hydrous peridotite with 1400 °C to 1250 °C potential temperature and an initial water content of 700 ppm; green dashed lines refer to an anhydrous harzburgite with 1550 °C to 1450 °C potential temperature. The melting degree of the mantle source is indicated with the same colour of the curves. We assumed an extension rate of 1.5 cm/year, a columnar melting zone and a pre-existing lithospheric thickness of 70 km. Green fields: data for Brixen and nearby gabbros from Visonà (1995). The light blue line represents Dy/Yb vs La/Yb variation for 0 to 50% fractional crystallization. b) REEBOX modelling for the hydrous peridotite with 1400 °C to 1250 °C potential temperature in terms of Zr/Nb vs La/Yb variation. (For interpretation of the references to colour in this figure legend, the reader is referred to the web version of this article.)

Table 6
Input parameters for REEBOX model.

	Spreading Rate (cm/yr)	Pre-existing lithosphere (km)	Water content (ppm)	Mantle Potential Temperatures (°C)	Ambient Mantle Potential Temperatures (°C)	Initial trace element compositions (ppm)	Reference
Hydrous Peridotite	1.5	70	700	1250; 1300; 1350; 1450	1250; 1300; 1350; 1450	DMM	Salters and Stracke (2004)
Harzburgite	1.5	70	–	1450; 1500; 1550	1450; 1500; 1550	Depleted DMM	Workman and Hart (2005)

Rb, Sr, K, Ba and Pb, which are all mobile in fluids and concentrated in subduction magmas (Kessel et al., 2005).

Further constraints on the mantle sources of the basic calc-alkaline dykes are provided by isotopic and trace element relationships. $^{143}Nd/^{144}Nd_i$ and $^{206}Pb/^{204}Pb_i$ are negatively correlated and are positively and inversely correlated (respectively) to Zr/Nb (and Hf/Ta). REEBOX modelling shows that increasing Zr/Nb may be related to slightly increasing degree of mantle melting (Fig. 14b), as Nb is more incompatible than Zr (Sun and McDonough, 1989). Generally, high $^{143}Nd/^{144}Nd_i$ (and low $^{206}Pb/^{204}Pb_i$) would suggest a relatively depleted mantle source, while low $^{143}Nd/^{144}Nd_i$ (and high $^{206}Pb/^{204}Pb_i$) would indicate a relatively enriched mantle source. Therefore, the Zr/Nb, $^{143}Nd/^{144}Nd_i$ and $^{206}Pb/^{204}Pb_i$ variability displayed by the calc-alkaline samples (Fig. 9c, d and 10d) could represent slightly variable melting degrees (ca. 1–4%; Fig. 14a) of a variably metasomatized mantle source. In such scenario, low degree melts would preferentially tap the enriched component, which are then diluted at higher degrees of melting.

An altogether different source is required for the tholeiitic samples AB14 and AB15. On trace element diagrams, these tholeiitic samples plot in the MORB fields (Fig. 11a, b). They also lack major HFSE negative anomalies (Fig. 8a), while they are relatively depleted in LREE compared to MREE (e.g., $La/Sm_{CN} < 1$), resembling N-MORBs (Hofmann, 1988; Sun and McDonough, 1989). Such geochemical features suggest derivation from a predominantly depleted mantle source (e.g., Zheng, 2019 and references therein) rather than a subduction-related enriched mantle source. Accordingly, the Ajaccio tholeiites also yield low Sr and high Nd isotopic compositions and plot towards the Depleted MORB Mantle field (Fig. 9a). Nevertheless, they are relatively enriched in Pb and yield relatively high Pb isotopic compositions (Fig. 9b, c), suggesting a minor subduction-like signature (i.e., small degrees of metasomatism) or small degree of mixing with the enriched mantle source that issued the calc-alkaline suite.

The mantle source of Brixen gabbros is difficult to constrain, due to the heavy overprint associated with crustal assimilation. Despite this, Brixen gabbros display whole-rock and calculated melt trace element compositions in many ways similar to the calc-alkaline Ajaccio dykes, likely indicating a subduction-related signature (Fig. 8b, c). They also plot in the calc-alkaline field (Fig. 11a) and towards the Enriched Mantle poles. In general, a calc-alkaline parental magma and thus an enriched source is likely for the Brixen gabbros.

8.5. Early Permian basic magmatism in the Southern Variscan Realm

Calc-alkaline dykes in the region of Ajaccio and the Brixen gabbroic complex included in this study show a common subduction-like signature. Such signature is also shared by numerous coeval Early Permian mafic intrusions throughout the Corsica-Sardinia batholith (Fig. 1a), e.g., the Porto complex (Renna et al., 2006, 2007), the gabbroic complex of Bocca di Tenda (Tribuzio et al., 2009), dykes from NW Corsica (Buraglini and Traversa, 2000), and tholeiitic to transitional basaltic dykes from central to southern Corsica and northern Sardinia (Traversa et al., 2003) (Fig. S3 in supplementary material). Apart from the Brixen gabbroic complex, Early Permian post-Variscan magmatism is also widespread in the Alps, such as the Mafic Formation in the Ivrea-Verbano Zone (e.g., Peressini et al., 2007; Sinigoi et al., 2016; Zanetti et al., 2013), the Sondalo gabbroic complex (e.g., Petri et al., 2017; Tribuzio et al., 1999) and Mt. Collon (e.g., Monjoie et al., 2005, 2007). In particular, Brixen, Mont Collon, Tenda and Porto gabbroic complexes display comparable whole-rock and clinopyroxene trace element compositions, yielding similar subduction-related signatures and thus supporting the hypothesis of subduction-enriched mantle being present on a regional scale as the main source for this magmatism (Fig. S3 in supplementary material). Moreover, calc-alkaline, transitional to tholeiitic dykes with slight HFSE-enrichment and alkaline basaltic dykes (Traversa et al., 2003) are located in southern Corsica and northern Sardinia. According to those authors, the transitional to tholeiitic dykes represent the shift from post-collisional magmatism (still yielding a marked subduction-related signature) to an anorogenic phase characterized by within-plate Late Permian-Early Triassic alkaline basaltic dykes.

In terms of Sr-Nd isotopic compositions, the Ajaccio dykes overlap in composition with other Permian south-Alpine mafic complexes (Fig. 12a). In particular, the Ajaccio tholeiites overlap with gabbros from the deep crust of the Permian Ivrea mafic bodies (Val Sesia; Voshage et al., 1990; Sinigoi et al., 2016 and references therein), while the calc-alkaline Ajaccio suite overlaps with other basic dykes and gabbros from Corsica, with Ivrea ultramafic pipes (Garuti et al., 2001) and with partially hybridized (i.e., crustally contaminated) gabbros from the upper part of the Ivrea zone (Sinigoi et al., 2016; Voshage et al., 1990). In terms of Pb isotopic compositions, they overlap with mafic rocks from the Ivrea-Verbano area (Fig. 12b, c; Cumming et al., 1987). The Brixen gabbro rocks, being the most crustally contaminated, overlap with the crustally contaminated rocks from Ivrea (Sinigoi et al., 2016) and plot close to silicic volcanic and plutonic Permian rocks from the Southern Alps (e.g. Rottura et al., 1998; Fig. 12a). However, they have the highest Pb isotopic composition among the Permian mafic rocks throughout the Corsica batholith and the Alps (Fig. 12b, c).

8.6. Geodynamic significance of Permian magmatism in southern and western Europe

Overall, based on our new trace element and Sr-Nd-Pb isotopic compositions, coupled with mantle-melting modelling, a heterogeneous mantle is preferred as the source of the post-orogenic magmatism that affected the Corsica batholith during the Early Permian. The calc-alkaline dykes may represent partial melting of mantle portions enriched by metasomatizing fluids released from crustal material subducted during the Variscan orogenic cycle. In contrast, the tholeiitic dykes may represent melting of a less enriched to depleted mantle which rose from greater depth at higher temperature than the mantle that sourced the calc-alkaline magmas. Likely, mixing of melts and minor crustal assimilation occurred during ascent and intrusion at shallow crustal levels. The Brixen gabbros are probably the most heavily contaminated magmas studied here, however, they still seem to share mantle source characteristics with the Ajaccio calc-alkaline suite.

Mantle partial melting in post-collisional settings is usually related to extensional tectonics, thinning of the lithosphere and partial melting of the rising asthenosphere (Bonin et al., 1998). Magmatism in late to post-collisional environments could also be enhanced by slab detachment (Ferrari, 2004), slab roll-back (Singer et al., 2014) and poloidal and toroidal mantle-flow (Brombin et al., 2019; Faccenna et al., 2011). In general, these geodynamic scenarios lead to uprising mantle from greater depths and to decompression melting. We speculate that decompression melting affected initially shallow portions of the former mantle wedge, which still retained the geochemical fingerprint of the Variscan subduction event(s). Subsequent partial melting may have formed the tholeiites, which were dominantly sourced from a depleted mantle rising from greater depths.

The geodynamic context, as well as similar geochemical compositions suggest that similar mantle melting scenarios may be applicable to the entire South European Permian magmatic suite. All of these basic magmas were emplaced in extensional environments (Rottura et al., 1998), but at least parts of them still yield a clear fingerprint of the subduction-modified mantle source.

8.7. Concluding remarks on the Permian to Triassic evolution of the Variscan domain

The enriched geochemical signatures observed in the Permian magmatism are also observed in subsequent magmatic events, which occurred at the edge of the former Variscan belt. During the Middle-Late Triassic, magmatic activity developed in the Southern Alps, Dinarides and Australpine domains with dominant basaltic rocks bearing a subduction

signature, despite the fact that these magmas are associated with an extensional setting (De Min et al., 2020; Lustrino et al., 2019 and references therein). Triassic magmas have similar trace element compositions compared to the Permian magmatism studied here, resembling a subduction-related signature (Fig. S3i, j in the supplementary material). However, the Triassic magmas are in general more enriched than the Permian magmas, as shown by their enrichment in K and by their Sr-Nd isotopic compositions trending to more enriched values (high Sr and low Nd isotopic compositions; Fig. 12a; Lustrino et al., 2019, and references therein). In particular, samples with a dominant DMM signature are missing among the mid-Triassic magmas, whose most depleted compositions are represented by lamprophyres, which are probable lithospheric mantle melts (De Min et al., 2020). Triassic magmas also yield similar to higher Pb isotopic compositions than the Ajaccio mafic dykes (overlapping with the Brixen gabbro; Fig. 12b, c).

At the very end of the Triassic, tholeiitic basalts were emplaced over central Pangea, forming the CAMP (Marzoli et al., 2019 and references therein). Basaltic magmas from this province also yield a significantly enriched subduction-related geochemical signature (Fig. S3k, l in the supplementary material), e.g. with higher Sr and lower Nd isotopic composition compared to the Ajaccio dykes or to the Ladinian magmas (Fig. 12a; Callegaro et al., 2014; Cebriá et al., 2003; Lustrino et al., 2019; Marzoli et al., 2019), but lower Pb isotopic compositions (Fig. 12b, c). The subduction fingerprint detected in CAMP basalts is probably due to recycled continental material from Paleozoic subduction events in the mantle source. The general development of post-Variscan magmatism during the Permian (e.g., the Permian basic magmas studied here) to the late Triassic (Carnian magmatism and then CAMP) highlights the importance of the Variscan orogeny in modifying the composition of the shallow mantle domains, probably favouring melting of more fertile mantle, enriched in incompatible trace element and possibly in volatiles.

9. Conclusions

New zircon U-Pb ages constrain the emplacement of a dyke swarm in the region of Ajaccio (Corsica) and of the Brixen gabbroic complex (Northern Italy) at ca. 282 Ma, i.e., at the end of the Variscan orogenic cycle. Calc-alkaline Ajaccio dykes display subduction-like signature, likely resulting from melting of an enriched mantle source rather than crustal assimilation, while minor tholeiitic dykes tapped a more depleted mantle source which originated from greater depths and temperature. The age of the tholeiites is not constrained here, but the most likely interpretation is that also their age is similar to those Permian tholeiites found in the Ivrea zone, Val Malenco or in Corsica and Sardinia. However, we can not exclude that the tholeiitic dykes may be somewhat younger than the calc-alkaline ones, thus representing a different pulse of the post-Variscan magmatism. Brixen gabbros show similar geochemical signatures to the calc-alkaline Ajaccio dykes, but record higher amounts of crustal assimilation.

Coeval mafic Permian magmatism throughout the Corsica-Sardinia batholith and the Southern Alps share common geochemical features, suggesting the presence of a heterogeneous mantle on a regional scale in the southern Variscan domain during the post-collisional evolution of the Variscan belt. The geodynamic context, as well as similar geochemical compositions suggest that similar mantle melting scenarios may be applicable to the entire South European Permian magmatic suite. Post-collisional magmatism is commonly explained by the collapse of the orogenic belt associated with an extensional tectonic phase, but other processes are likely to enhance mantle-melting, such as slab detachment, slab roll-back, and poloidal as well as toroidal mantle flow, which may generate magmatism millions of years after the main collisional event.

The subduction-like signature recognized in the Ajaccio and Brixen Permian magmatism is still observed in the subsequent mid-Triassic magmatism throughout the western Tethys and Late-Triassic CAMP magmatism, suggesting that shallow mantle modified by fertile crustal material during subductions may be a critical factor for enhancing mantle melting during post-collisional evolution of orogenic belts.

Declaration of Competing Interest

The authors declare that they have no known competing financial interests or personal relationships that could have appeared to influence the work reported in this paper.

Acknowledgments

We thank R. Carampin and D. Pasqual (IGG-CNR and University of Padova) for support during EMP and XRF analyses, A. Ulyanov (Lausanne) for support during LA-ICP-MS analyses, M. Senn (Geneva) for precious analytical support. Financial support was provided by PRIN-2017 (Italian PRIN 20178LPCP to AM, ADM and AZ). Constructive reviews of C. Rogers and an anonymous reviewer helped us to improve the early version of the manuscript.

Appendix A. Supplementary data

Supplementary data to this article can be found online at https://doi.org/10.1016/j.lithos.2020.105733.

References

Aigner-Torres, M., Blundy, J., Ulmer, P., Pettke, T., 2007. Laser Ablation ICPMS study of trace element partitioning between plagioclase and basaltic melts: an experimental approach. Contrib. Mineral. Petrol. 153, 647–667. https://doi.org/10.1007/s00410-006-0168-2.

Barrat, J.A., Keller, F., Amossé, J., Taylor, R.N., Nesbitt, R.W., Hirata, T., 1996. Determination of rare earth elements in sixteen silicate reference samples by ICP-MS after TM addition and ion exchange separation. Geostand. Newslett. 20, 133–139. https://doi.org/10.1111/j.1751-908X.1996.tb00177.x.

Béguelin, P., Chiaradia, M., Beate, B., Spikings, R., 2015. The Yanaurcu volcano (Western Cordillera, Ecuador): a field, petrographic, geochemical, isotopic and geochronological study. Lithos 218–219, 37–53. https://doi.org/10.1016/j.lithos.2015.01.014.

Bellieni, G., Fioretti, A.M., Marzoli, A., Visonà, D., 2010. Permo-Paleogene magmatism in the eastern Alps. Rendiconti Lincei 21, 51–71. https://doi.org/10.1007/s12210-010-0095-z.

Bohrson, W.A., Spera, F.J., 2001. Energy-Constrained Open-System Magmatic Processes II: Application of Energy-Constrained Assimilation-Fractional Crystallization (EC-AFC) Model to Magmatic Systems. J. Petrol. 42, 1019–1041. https://doi.org/10.1093/petrology/42.5.1019.

Bonin, B., Azzouni-Sekkal, A., Bussy, F., Ferrag, S., 1998. Alkali-calcic and alkaline post-orogenic (PO) granite magmatism: Petrologic constraints and geodynamic settings. Lithos 45, 45–70. https://doi.org/10.1016/S0024-4937(98)00025-5.

Brombin, V., Bonadiman, C., Jourdan, F., Roghi, G., Coltorti, M., Webb, L.E., Callegaro, S., Bellieni, G., De Vecchi, G., Sedea, R., Marzoli, A., 2019. Intraplate magmatism at a convergent plate boundary: the case of the Cenozoic northern Adria magmatism. Earth Sci. Rev. 192, 355–378. https://doi.org/10.1016/j.earscirev.2019.03.016.

Brown, E.L., Lesher, C.E., 2016. REEBOX PRO: a forward model simulating melting of thermally and lithologically variable upwelling mantle. Geochem. Geophys. Geosyst. 17, 3929–3968. https://doi.org/10.1002/2016GC006579.

Buraglini, N., Traversa, G., 2000. Petrology and mineral chemistry of late-Hercynian dykes from NW Corsica (France). Periodico Mineral. 69, 269–310.

Callegaro, S., Rapaille, C., Marzoli, A., Bertrand, H., Chiaradia, M., Reisberg, L., Bellieni, G., Martins, L., Madeira, J., Mata, J., Youbi, N., De Min, A., Azevedo, M.R., Bensalah, M.K., 2014. Enriched mantle source for the Central Atlantic magmatic province: New supporting evidence from southwestern Europe. Lithos 188, 15–32. https://doi.org/10.1016/j.lithos.2013.10.021.

Carmignani, L., Rossi, P., 2000. Carta Geologica e Strutturale della Sardegna e della Corsica – Carte Géologique et Structurale de la Corse et de la Sardaigne. Scale 1: 500.000 – Servizio Geologico d'Italia. BRGM Service Géologiques Nationale.

Casetta, F., Coltorti, M., Ickert, R.B., Bonadiman, C., Giacomoni, P.P., Ntaflos, T., 2018. Intrusion of shoshonitic magmas at shallow crustal depth: T-P path, H_2O estimates, and AFC modelling of the Middle Triassic Predazzo Intrusive complex (Southern Alps, Italy). Contrib. Mineral. Petrol. 173.

Cassinis, G., Toutin-Morin, N., Virgili, C., 1995. A General Outline of the Permian Continental Basins in Southwestern Europe, in: The Permian of Northern Pangea. Springer, Berlin Heidelberg, pp. 137–157. https://doi.org/10.1007/978-3-642-78590-0_8.

Cassinis, G., Perotti, C.R., Ronchi, A., 2012. Permian continental basins in the Southern Alps (Italy) and peri-mediterranean correlations. Int. J. Earth Sci. 101, 129–157. https://doi.org/10.1007/s00531-011-0642-6.

Cebriá, J.M., López-Ruiz, J., Doblas, M., Martíns, L.T., Munha, J., 2003. Geochemistry of the Early Jurassic Messejana-Plasencia dyke (Portugal-Spain); Implications on the origin of the Central Atlantic Magmatic Province. J. Petrol. 44, 547–568.

Chiaradia, M., Müntener, O., Beate, B., 2011. Enriched basaltic andesites from mid-crustal fractional crystallization, recharge, and assimilation (Pilavo volcano, Western Cordillera of Ecuador). J. Petrol. 52, 1107–1141. https://doi.org/10.1093/petrology/egr020.

Cocherie, A., Rossi, P., Fouillac, A.M., Vidal, P., 1994. Crust and mantle contributions to granite genesis - an example from the Variscan batholith of Corsica, France, studied by trace-element and NdSrO-isotope systematics. Chem. Geol. 115, 173–211. https://doi.org/10.1016/0009-2541(94)90186-4.

Cocherie, A., Rossi, P., Fanning, C.M., Guerrot, C., 2005. Comparative use of TIMS and SHRIMP for U-Pb zircon dating of A-type granites and mafic tholeiitic layered complexes and dykes from the Corsican Batholith (France). Lithos 82, 185–219. https://doi.org/10.1016/j.lithos.2004.12.016.

Cumming, G.L., Köppel, V., Ferrario, A., 1987. A lead isotope study of the northeastern Ivrea Zone and the adjoining Ceneri zone (N-Italy): evidence for a contaminated subcontinental mantle. Contrib. Mineral. Petrol. 97, 19–30.

Davies, J.H., von Blanckenburg, F., 1995. Slab break-off: a model of lithosphere detachment and its test in the magmatism and deformation of collisional orogens. Earth Planet. Sci. Lett. 129, 85–102.

Davies, J.H.F.L., Marzoli, A., Bertrand, H., Youbi, N., Ernesto, M., Schaltegger, U., 2017. End-Triassic mass extinction started by intrusive CAMP activity. Nat. Commun. https://doi.org/10.1038/NCOMMS15596.

De Min, A., Velicogna, M., Ziberna, L., Chiaradia, M., Alberti, A., Marzoli, A., 2020. Triassic magmatism in the European Southern Alps as an early phase of Pangea break-up. Geol. Mag., 1–23 https://doi.org/10.1017/S0016756820000084.

Del Moro, A., Visonà, D., 1982. The epiplutonic Hercynian complex of Bressanone (Brixen, Eastern Alps, Italy). Petrologic and radiometric data. Neues Jahrbuch für Mineralogie 145, 66–85.

Denyszyn, S.W., Fiorentini, M.L., Maas, R., Dering, G., 2018. A bigger tent for CAMP. Geology 46, 823–826.

Dokuz, A., Aydin, F., Karslı, O., 2019. Postcollisional transition from subduction- to intraplate-type magmatism in the eastern Sakarya zone, Turkey: Indicators of northern Neotethyan slab breakoff. Geol. Soc. Am. Bull. 131, 1623–1642. https://doi.org/10.1130/b31993.1.

Faccenna, C., Molin, P., Orecchio, B., Olivetti, V., Bellier, O., Funiciello, F., Minelli, L., Piromallo, C., Billi, A., 2011. Topography of the Calabria subduction zone (southern Italy): Clues for the origin of Mt. Etna. Tectonics 30. https://doi.org/10.1029/2010TC002694.

Faure, M., Bé Mézème, E., Duguet, M., Cartier, C., Talbot, J.Y., 2005. Paleozoic tectonic evolution of medio-Europa from the example of the French Massif Central and Massif Armoricain. J. Virtual Explor. 19. https://doi.org/10.3809/jvirtex.2005.00120.

Ferrari, L., 2004. Slab detachment control on mafic volcanic pulse and mantle heterogeneity in Central Mexico. Geology 32, 77–80. https://doi.org/10.1130/G19887.1.

Fiorentini, M.L., LaFlamme, C., Denyszyn, S., Mole, D., Maas, R., Locmelis, M., Caruso, S., Bui, T., 2018. Post-collisional alkaline magmatism as gateway for metal and sulfur enrichment of the continental lower crust. Geochim. Cosmochim. Acta 223, 175–197.

Froitzheim, N., Derks, J.F., Walter, J.M., Sciunnach, D., 2008. Evolution of an early Permian extensional detachment fault from syntrusive, mylonitic flow to brittle faulting (Grassi Detachment Fault, Orobic Anticline, southern Alps, Italy). In: Siegmund, S., Fügenschuh, B., Froitzheim, N. (Eds.), Tectonic Aspects of the Alpine-Dinaride-Carpathian System. 298. Geological Society, London, Special Publication, pp. 69–82. https://doi.org/10.1144/SP298.4.

Garuti, G., Bea, F., Zaccarini, F., Montero, P., 2001. Age, geochemistry and petrogenesis of the ultramafic pipes in the Ivrea Zone, NW Italy. J. Petrol. 42, 433–457. https://doi.org/10.1093/petrology/42.2.433.

Guo, Z., Wilson, M., Zhang, M., Cheng, Z., Zhang, L., 2015. Post-collisional ultrapotassic mafic magmatism in South Tibet: Products of partial melting of pyroxenite in the mantle wedge induced by roll-back and delamination of the subducted Indian continental lithosphere slab. J. Petrol. 56, 1365–1406. https://doi.org/10.1093/petrology/egv040.

Hamilton, M.A., Pearson, D.G., 2011. Precise U-Pb Age for the Great Whin Dolerite complex, N.E. England and its significance. In: Srivastava, R.K. (Ed.), Dyke Swarms: Keys for Geodynamic Interpretation. Springer, Berlin, Heidelberg, pp. 495–507. https://doi.org/10.1007/978-3-642-12496-9_26.

Hart, S.R., 1984. A large-scale isotope anomaly in the Southern Hemisphere mantle. Nature 309, 753–757. https://doi.org/10.1038/309753a0.

Heeremans, M., Timmerman, M.J., Kirstein, L.A., Faleide, J.I., 2004. New constraints on the timing of late Carboniferous-early Permian volcanism in the Central North Sea. Geol. Soc. Spec. Publ. 223, 177–194. https://doi.org/10.1144/GSL.SP.2004.223.01.08.

Hermann, J., Müntener, O., Günther, D., 2001. Differentiation of mafic magma in a continental crust-to-mantle transition zone. J. Petrol. 42, 189–206.

Hill, E., Wood, B.J., Blundy, J.D., 2000. The effect of Ca-Tschermaks component on trace element partitioning between clinopyroxene and silicate melt. Lithos 53, 203–215. https://doi.org/10.1016/S0024-4937(00)00025-6.

Hoffmann, U., Breitkreuz, C., Breiter, K., Sergeev, S., Stanek, K., Tichomirowa, M., 2013. Carboniferous-Permian volcanic evolution in Central Europe-U/Pb ages of volcanic rocks in Saxony (Germany) and northern Bohemia (Czech Republic). Int. J. Earth Sci. 102, 73–99. https://doi.org/10.1007/s00531-012-0791-2.

Hofmann, A.W., 1988. Chemical differentiation of the Earth: the relationship between mantle, continental crust, and oceanic crust. Earth Planet. Sci. Lett. 90, 297–314. https://doi.org/10.1016/0012-821X(88)90132-X.

Hollocher, K., Robinson, P., Walsh, E., Roberts, D., 2012. Geochemistry of amphibolite-facies volcanics and gabbros of the støren nappe in extensions west and southwest of Trondheim, Western Gneiss Region, Norway: a key to correlations and paleotectonic settings. Am. J. Sci. 312, 357–416. https://doi.org/10.2475/04.2012.01.

Irvine, T.N., Baragar, W.R.A., 1971. A Guide to the Chemical Classification of the Common Volcanic Rocks. Can. J. Earth Sci. 8, 523–548. https://doi.org/10.1139/e71-055.

Johnson, M.C., Plank, T., 1999. Dehydration and melting experiments constrain the fate of subducted sediments. Geochem. Geophys. Geosyst. 1.

Kessel, R., Schmidt, M.W., Ulmer, P., Pettke, T., 2005. Trace element signature of subduction-zone fluids, melts and supercritical liquids at 120-180 km depth. Nature 437, 724–727. https://doi.org/10.1038/nature03971.

Klötzli, U.S., Sinigoi, S., Quick, J.E., Demarchi, G., Tassinari, C.C.G., Sato, K., Günes, Z., 2014. Duration of igneous activity in the Sesia Magmatic System and implications for high-temperature metamorphism in the Ivrea-Verbano deep crust. Lithos 206-207, 19–33.

Läufer, A.L., Hubich, D., Loeschke, J., 2001. Variscan geodynamic evolution of the Carnic Alps (Austria/Italy). Int. J. Earth Sci. 90, 855–870. https://doi.org/10.1007/s005310100194.

Le Bas, M.J., Le Maitre, R.N., Streckeisen, A., Zanettin, B., 1986. A chemical classification of volcanic rock based on total silica diagram. J. Petrol. 27, 745–750.

Locock, A.J., 2014. An Excel spreadsheet to classify chemical analyses of amphiboles following the IMA 2012 recommendations. Comput. Geosci. 62, 1–11. https://doi.org/10.1016/j.cageo.2013.09.011.

Lustrino, M., Abbas, H., Agostini, S., Caggiati, M., Carminati, E., Gianolla, P., 2019. Origin of Triassic magmatism of the Southern Alps (Italy): Constraints from geochemistry and Sr-Nd-Pb isotopic ratios. Gondwana Res. 75, 218–238. https://doi.org/10.1016/j.gr.2019.04.011.

Marocchi, M., Morelli, C., Mair, V., Klötzli, U., Bargossi, G.M., Bologna, U., 2008. Evolution of large Silicic Magma Systems: New U-Pb Zircon Data on the NW Permian Athesian Volcanic Group (Southern Alps, Italy). J. Geol. 116, 480–498. https://doi.org/10.1086/590135.

Marzoli, A., Bertrand, H., Youbi, N., Callegaro, S., Merle, R., Reisberg, L., Chiaradia, M., Brownlee, S.I., Jourdan, F., Zanetti, A., Davies, J.H.F.L., Cuppone, T., Mahmoudi, A., Medina, F., Renne, P.R., Bellieni, G., Crivellari, S., El Hachimi, H., Bensalah, M.K., Meyzen, C.M., Tegner, C., 2019. The Central Atlantic Magmatic Province (CAMP) in Morocco. J. Petrol. 60, 945–996. https://doi.org/10.1093/petrology/egz021.

Matte, P., 2001. The Variscan collage and orogeny (480–290 Ma) and the tectonic definition of the Armorica microplate: a review. Terra Nova 13, 122–128.

McDonough, W.F., Sun, S.S., 1995. The composition of the Earth. Chem. Geol. 120, 223–253. https://doi.org/10.1016/0009-2541(94)00140-4.

Miller, C., Zanetti, A., Thöni, M., Konzett, J., Klötzli, U.S., 2012. Mafic and silica-rich glasses in mantle xenoliths from Wau-en-Namus, Libya: textural and geochemical evidence for peridotite–melt reactions. Lithos 128-131, 11–26.

Monjoie, P., Bussy, F., Lapierre, H., Pfeifer, H.R., 2005. Modelling of in-situ crystallization processes in the Permian mafic layered intrusion of Mont Collon (Dent Blanche nappe, western Alps). Lithos 83, 317–346. https://doi.org/10.1016/j.lithos.2005.03.008.

Monjoie, P., Bussy, F., Schaltegger, U., Mulch, A., Lapierre, H., Pfeifer, H.R., 2007. Contrasting magma types and timing of intrusion in the Permian layered mafic complex of Mont Collon (Western Alps, Valais, Switzerland): evidence from U/Pb zircon and $^{40}Ar/^{39}Ar$ amphibole dating. Swiss J. Geosci. 100, 125–135. https://doi.org/10.1007/s00015-007-1210-8.

Morimoto, N., Fabries, J., Ferguson, A.K., Ginzburg, I.V., Ross, M., Seifert, F.A., Zussman, J., 1988. Nomenclature of Pyroxenes. Mineral. Mag. 52, 535–550.

Muttoni, G., Kent, D.V., Garzanti, E., Brack, P., Abrahamsen, N., Gaetani, M., 2003. Early Permian Pangea "B" to Late Permian Pangea "A.". Earth Planet. Sci. Lett. 215, 379–394. https://doi.org/10.1016/S0012-821X(03)00452-7.

Neumann, E.R., Wilson, M., Heeremans, M., Spencer, E.A., Obst, K., Timmerman, M.J., Kirstein, L., 2004. Carboniferous-Permian rifting and magmatism in southern Scandinavia, the North Sea and northern Germany: A review. In: Wilson, M., Neumann, E.R., Davies, G.R., Timmerman, M.J., Heeremans, M., Larsen, B.T. (Eds.), Permo-Carboniferous Magmatism and Rifting in Europe. Geological Society, London, Special Publications 223, pp. 11–40.

Orsini, J.B., 1980. Le batholite corso-sarde: un exemple de batholite hercynien (structure, composition, organisation d'ensemble). University of Aix-Marseille III, Sa place dans la chaine varisque de l'Europe moyenne. Doctoral thesis, p. 370.

Paquette, J.L., Ménot, R.P., Pin, C., Orsini, J.B., 2003. Episodic and short-lived granitic pulses in a post-collisional setting: evidence from precise U-Pb zircon dating through a crustal cross-section in Corsica. Chem. Geol. 198, 1–20. https://doi.org/10.1016/S0009-2541(02)00401-1.

Pearce, J.A., 1983. Role of the Sub-continental Lithosphere in magma genesis at active continental margins. In: Hawkesworth, C.J., Norry, M.J. (Eds.), Continental Basalts and Mantle Xenoliths. Shiva, Nantwich, pp. 230–249.

Pereira, M.F., Castro, A., Chichorro, M., Fernández, C., Díaz-Alvarado, J., Martí, J., Rodríguez, C., 2014. Chronological link between deep-seated processes in magma chambers and eruptions: Permo-Carboniferous magmatism in the core of Pangaea (Southern Pyrenees). Gondwana Res. 25, 290–308. https://doi.org/10.1016/j.gr.2013.03.009.

Peressini, G., Quick, J.E., Sinigoi, S., Hofmann, A.W., Fanning, M., 2007. Duration of a large Mafic intrusion and heat transfer in the lower crust: a SHRIMP U-Pb zircon Study in the Ivrea-Verbano Zone (Western Alps, Italy). J. Petrol. 48, 1185–1218. https://doi.org/10.1093/petrology/egm014.

Petri, B., Mohn, G., Skrzypek, E., Mateeva, T., Galster, F., Manatschal, G., 2017. U–Pb geochronology of the Sondalo gabbroic complex (Central Alps) and its position within the Permian post-Variscan extension. Int. J. Earth Sci. 106, 2873–2893. https://doi.org/10.1007/s00531-017-1465-x.

Poilvet, J.C., Poujol, M., Pitra, P., Van Den Driessche, J., Paquette, J.L., 2011. The Montalet granite, Montagne Noire, France: an early Permian syn-extensional pluton as evidenced by new U-Th-Pb data on zircon and monazite. Comptes Rendus-Geosci. 343, 454–461. https://doi.org/10.1016/j.crte.2011.06.002.

Poitrasson, F., Paquette, J.L., Montel, J.M., Pin, C., Duthou, J.L., 1998. Importance of late-magmatic and hydrothermal fluids on the Sm-Nd isotope mineral systematics of hypersolvus granites. Chem. Geol. 146, 187–203. https://doi.org/10.1016/S0009-2541(98)00010-2.

Renna, M.R., Tribuzio, R., Tiepolo, M., 2006. Interaction between basic and acid magmas during the latest stages of the post-collisional Variscan evolution: Clues from the gabbro-granite association of Ota (Corsica-Sardinia batholith). Lithos 90, 92–110. https://doi.org/10.1016/j.lithos.2006.02.003.
Renna, M.R., Tribuzio, R., Tiepolo, M., 2007. Origin and timing of the post-Variscan gabbro-granite complex of Porto (Western Corsica). Contrib. Mineral. Petrol. 154, 493–517. https://doi.org/10.1007/s00410-007-0205-9.
Rey, P., Vanderhaeghe, O., Teyssier, C., 2001. Gravitational collapse of the continental crust: Definition, regimes and modes. Tectonophysics 342, 435–449. https://doi.org/10.1016/S0040-1951(01)00174-3.
Rogers, C., Mackinder, A., Ernst, R.E., Cousens, B., 2016. Mafic magmatism in the Belt-Purcell Basin and Wyoming Province of western Laurentia. In: Mac Lean, J.S., Sears, J.W. (Eds.), Belt Basin : Window to Mesoproterozoic Earth. Geological Society of America Special Paper 522, pp. 243–282.
Rossi, P., Cocherie, A., 1995. Chronologie des intrusions du batholite corse: données de l'évaporation du plomb sur monozircon. S.G.F.. Magmatismes dans le Sud-Est de la France. Nice 24, 25–27.
Rossi, P., Oggiano, G., Cocherie, A., 2009. A restored section of the "southern Variscan realm" across the Corsica-Sardinia microcontinent. Compt. Rendus Geosci. 341, 224–238. https://doi.org/10.1016/j.crte.2008.12.005.
Rottura, A., Bargossi, G.M., Caggianelli, A., Del Moro, A., Visonà, D., Tranne, C.A., 1998. Origin and significance of the Permian high-K calc-alkaline magmatism in the central-eastern Southern Alps, Italy. Lithos 45, 329–348. https://doi.org/10.1016/S0024-4937(98)00038-3.
Rudnick, R.L., Gao, S., 2003. The composition of the continental crust. In: Rudnick, R.L. (Ed.), The Crust. vol. 3. Elsevier, Amsterdam, pp. 1–64.
Salters, V.J.M., Stracke, A., 2004. Composition of the depleted mantle. Geochemistry, Geophysics, Geosystems 5.
Schaltegger, U., Brack, P., 2007. Crustal-scale magmatic systems during intracontinental strike-slip tectonics: U, Pb and Hf isotopic constraints from Permian magmatic rocks of the Southern Alps. Int. J. Earth Sci. 96, 1131–1151. https://doi.org/10.1007/s00531-006-0165-8.
Singer, J., Diehl, T., Husen, S., Kissling, E., Duretz, T., 2014. Alpine lithosphere slab rollback causing lower crustal seismicity in northern foreland. Earth Planet. Sci. Lett. 397, 42–56. https://doi.org/10.1016/j.epsl.2014.04.002.
Sinigoi, S., Quick, J.E., Demarchi, G., Klötzli, U.S., 2016. Production of hybrid granitic magma at the advancing front of basaltic underplating: Inferences from the Sesia Magmatic System (South-Western Alps, Italy). Lithos 252–253, 109–122. https://doi.org/10.1016/j.lithos.2016.02.018.
Soder, C.G., Romer, R.L., 2018. Post-collisional potassic-ultrapotassic magmatism of the Variscan orogen: implications for mantle metasomatism during continental subduction. J. Petrol. 59, 1007–1034.
Sun, S.S., McDonough, W.F., 1989. Chemical and isotopic systematics of oceanic basalts: Implications for mantle composition and processes. In: Saunders, A.D., Norry, M.J. (Eds.), Magmatism in the Ocean Basins. Geological Society, London, Special Publication 42, pp. 313–345.
Traversa, G., Ronca, S.S., Del Moro, A., Pasquali, C., Buraglini, N., Barabino, G., 2003. Late to post-Hercynian dyke activity in the Sardinia-Corsica Domain: a transition from orogenic calc-alkaline to anorogenic alkaline magmatism. Boll. Soc. Geol. Ital. 2, 131–152.
Tribuzio, R., Thirlwall, M.F., Messiga, B., 1999. Petrology, mineral and isotope geochemistry of the Sondalo gabbroic complex (Central Alps, Northern Italy): Implications for the origin of post-Variscan magmatism. Contrib. Mineral. Petrol. 136, 48–62. https://doi.org/10.1007/s004100050523.
Tribuzio, R., Renna, M.R., Braga, R., Dallai, L., 2009. Petrogenesis of early Permian olivine-bearing cumulates and associated basalt dykes from Bocca di Tenda (Northern Corsica): Implications for post-collisional Variscan evolution. Chem. Geol. 259, 190–203. https://doi.org/10.1016/j.chemgeo.2008.10.045.
Turner, S.P., Foden, J.D., Morrison, R.S., 1992. Derivation of some A-type magmas by fractionation of basaltic magma: an example from the Padthaway Ridge, South Australia. Lithos 28, 151–179. https://doi.org/10.1016/0024-4937(92)90029-X.
Ulianov, A., Müntener, O., Schaltegger, U., Bussy, F., 2012. The data treatment dependent variability of U-Pb zircon ages obtained using mono-collector, sector field, laser ablation ICPMS. J. Anal. At. Spectrom. 27, 663–676. https://doi.org/10.1039/c2ja10358c.
Van der Voo, R., 1993. Paleomagnetism of the Atlantic, Tethys and Iapetus Oceans. Cambridge University Press, Cambridge https://doi.org/10.1017/CBO9780511524936.
Visonà, D., 1995. Polybaric evolution of calc-alkaline magmas: the Dioritic Belt of the Bressanone-Chiusa Igneous complex (NE Italy). Memorie di Scienze Geologiche 47, 111–124.
Visonà, D., Fioretti, A.M., Poli, M.E., Zanferrari, A., Fanning, M., 2007. U-Pb SHRIMP zircon dating of andesite from the Dolomite area (NE Italy): geochronological evidence for the early onset of Permian Volcanism in the eastern part of the southern Alps. Swiss J. Geosci. 100, 313–324. https://doi.org/10.1007/s00015-007-1219-z.
Voshage, H., Hofmann, A.W., Mazzucchelli, M., Rivalenti, G., Sinigoi, S., Raczek, I., Demarchi, G., 1990. Isotopic evidence from the Ivrea Zone for a hybrid lower crust formed by magmatic underplating. Nature 347, 731–736.
Whitney, D.L., Teyssier, C., Rey, P., Roger Buck, W., 2013. Continental and oceanic core complexes. Bull. Geol. Soc. Am. https://doi.org/10.1130/B30754.1.
Wood, D.A., 1980. The application of a Th-Hf-Ta diagram to problems of tectonomagmatic classification and to establishing the nature of crustal contamination of basaltic lavas of the British Tertiary Volcanic Province. Earth Planet. Sci. Lett. 50, 11–30. https://doi.org/10.1016/0012-821X(80)90116-8.
Workman, R.K., Hart, S.R., 2005. Major and trace element composition of the depleted MORB mantle (DMM). Earth Planet. Sci. Lett. 231, 53–72.
Wyhlidal, S., Thöny, W.F., Tropper, P., Kaindl, R., Hauzenberger, C., Mair, V., 2012. Petrology of contact metamorphic metapelites from the southern rim of the Permian Brixen Granodiorite (South Tyrol, Italy). Mineral. Petrol. 106, 173–191. https://doi.org/10.1007/s00710-012-0240-8.
Zanetti, A., Mazzucchelli, M., Sinigoi, S., Giovanardi, T., Peressini, G., Fanning, M., 2013. SHRIMP U-Pb ZirconTriassic Intrusion Age of the Finero Mafic complex (Ivrea-Verbano Zone, Western Alps) and its Geodynamic Implications. J. Petrol. 54, 2235–2265. https://doi.org/10.1093/petrology/egt046.
Zheng, Y.F., 2019. Subduction zone geochemistry. Geosci. Front. 10, 1223–1254. https://doi.org/10.1016/j.gsf.2019.02.003.
Ziegler, A.M., Hulver, M.L., Rowley, D.B., 1997. Permian world topography and climate. In: Martini, I.P. (Ed.), Late Glacial and Postglacial Environmental Changes: Quaternary. Carboniferous– Permian and Proterozoic. Oxford Univ Press, Oxford, pp. 111–146.